energies

MDPI

*Review*

# Recent insights into low surface area catalysts for hydrogen production from ammonia

**Marina Pinzón [1], Paula Sánchez [1], Ana Raquel de la Osa [1], Amaya Romero [2] and Antonio de Lucas-Consuegra [1,*]**

[1] Department of Chemical Engineering, Faculty of Chemical Sciences and Technologies, University of Castilla-La Mancha, Avenida Camilo José Cela 12, 13071, Ciudad Real, Spain; marina.pgarcia@uclm.es (M.P.), paula.sanchez@uclm.es (P.S.), anaraquel.osa@uclm.es (A.R.d.l.O.)

[2] Department of Chemical Engineering, Higher Technical School of Agronomical Engineers, University of Castilla-La Mancha, Ronda de Calatrava 7, 13071, Ciudad Real, Spain; amaya.romero@uclm.es (A.R.)

* Correspondence: antonio.lconsugra@uclm.es (A.d.L.-C.)

**Abstract:** A potential source to storage and transport hydrogen safely in a cost-effectively practical way comprises the utilization of molecules that contains hydrogen in its structure such as ammonia. Because of high hydrogen content, mature technology (easy liquefaction) and carbon-free molecule, ammonia has gained attention as 'hydrogen carrier' to generate energy. Unfortunately, hydrogen production from ammonia requires an efficient catalyst to achieve high conversion at low reaction temperatures. Recently, very attractive results have been obtained with low surface area materials. This review paper is focused on summarizing and comparing recent advances in novel, economic and active catalysts for this reaction, paying particular attention to materials with low surface area as silicon carbide (SiC) or perovskites ($ABO_3$ structure). The effect of the supports, the active phase and the addition of promoters have been analyzed in detail in such low porous materials. Advances of adequate catalytic systems (including support and active metal) benefit the ammonia perspective as hydrogen carrier for the decarbonization of the energy sector and accelerate the 'hydrogen economy'.

**Keywords:** Hydrogen production; Ammonia decomposition; Catalysts; Low surface area; Ruthenium; nickel; cobalt; novel support

**Citation:**

Academic Editor:

Received: date
Accepted: date
Published: date



## 1. Introduction

A great deal effort is made by the scientific community to identify new energy sources and vectors to replace the fossil fuels through the decarbonization of the energy sector [1,2]. Despite of solar, wind and hydroelectricity technologies are consolidated as renewable energy sources, they suffer intermittency due to weather conditions.

Green hydrogen ($H_2$), produced from ecofriendly resources, might resolve the massively energy storage required to mitigate the fluctuations of these energies and meet the global energy demand [3]. The concept of using hydrogen as an energy carrier dates back to more than two centuries ago. However, until the energy crisis of the 70s, its growth was not accentuated. After that, numerous advances were achieved in this field in the 80s [4].

Hydrogen is a renewable, clean, and non-toxic fuel that, when it is combusted, only releases energy and vapor water into the atmosphere [5]. It does not present spillage problems, as it disperses quickly (due to its very low density), and it has much more chemical energy per mass than any fuel made from hydrocarbons. Its energy content is very high (141.9 MJ $kg^{-1}$) and very low in volume, showing that it is an adequate carrier of energy. Therefore, hydrogen, instead of being a source of energy, it stores energy and delivers it in a usable form and it is the most abundant element in the universe [6]. Additionally, it yields twice the electricity generation of conventional fossil fuels [7].

In this context, it is known as 'hydrogen economy' the system that tries to satisfy the society energy needs through hydrogen, instead of using fossil fuels. The hydrogen economy would provide a lasting response to the triple challenge that the world currently faces, meeting the energy needs of emerging countries, the depletion of fossil resources, and the threat of the consequences of Climate Change [8]. Despite the enormous advantages of establishing this system, its success depends on the development of five key elements: production, delivery, storage, conversion, and applications of hydrogen.

Nonetheless, only a small part of the generated $H_2$ is applied for energy purposes, whereas the 92% of $H_2$ is used as a chemical feedstock and in the metallurgical and petrochemical industries [9].

Currently, 70 $Mt_{H2}$ per year are demanded (International Energy Agency) by industrial processes, which the most $H_2$ generation relies on the steam-methane reforming. However, this technique generates about 7 kg of $CO_2$ per kg of $H_2$ [10] and must be replaced by processes using environmentally friendly routes to reach the net zero carbon emission.

However, the success of the hydrogen economy and the use of this compound as an energy carrier depends on the current $H_2$ storage and transport routes, which are characterized by their high costs (high pressure or low temperature) [11]. A potential solution to this issue comprises the utilization of molecules that contains hydrogen in their structure ('$H_2$ carriers'), which have been explored for storing $H_2$ safely and in an economically feasible way, so it is possible to transport it using current supply networks [12,13].

## 2. Roles of ammonia in a hydrogen economy

Among the substances capable of assuming the role of $H_2$ carriers (methane, formic acid, derivates of amines, ammonia and complex hydrides), ammonia ($NH_3$) should be highlighted.

Ammonia market involves a mature technology (it is the second most-produced chemical globally), a relatively low cost of production, storage and distribution using existing rail, road, marine and pipeline networks [14–18]. This compound can be easily liquefied under 8.6 bar and 20 °C, so that, this procedure consumes less energy than liquid hydrogen (-253 °C at 1 bar), and its vessels and pipes are light and easy to design [19]. Besides, it is a non-flammable, non-dangerous and easily detectable substance. Because of all this, along with the fact that it allows to produce 121 kg of $H_2$ per $m^3$ of $NH_3$, which is the double than that produced by liquid hydrogen (71 kg of $H_2$ per $m^3$ of liquid $H_2$) and that it is a carbon-free molecule, ammonia is considered an excellent $H_2$ carrier to mitigate issues related to the storage and transport of hydrogen [20,21]. In addition, $NH_3$ can help in the transition toward a clean future as viable fuel, so it can be directly used thermochemically (combustion), thermal decomposition (ammonia decomposition) and/or electro-chemically (fuel cells), as summarized in Figure 1 [16,19,21–23].

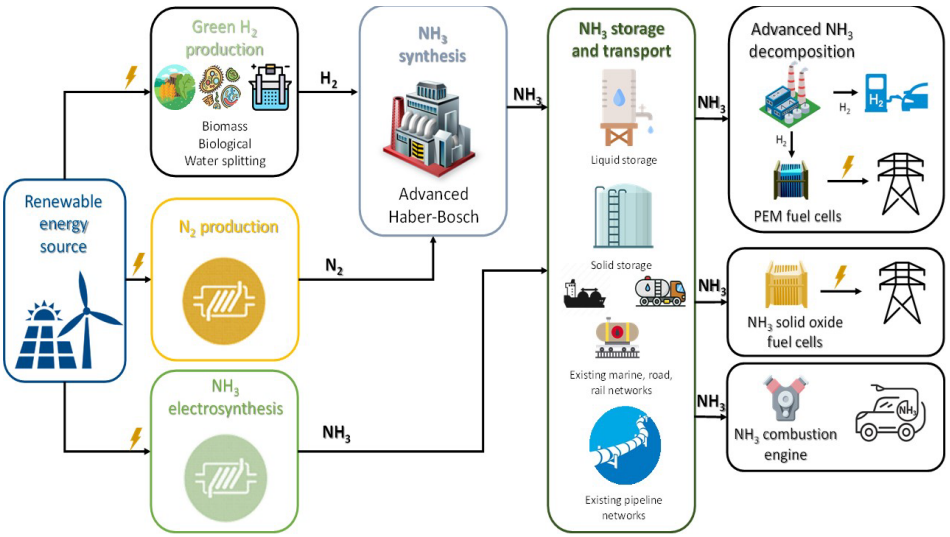


**Figure 1.** Roles of ammonia in a hydrogen economy. Adapted with permission [22]. Copyright 2021, Elsevier.

Ammonia is usually produced in large quantities (180 Mt annually) through the catalytic reaction of hydrogen and nitrogen at temperatures around 400-600 °C and pressures around 200-400 atmospheres (Haber-Bosch process). These raw materials come from air and hydrogen separating plants. To reduce the carbon footprint of the Haber-Bosch process a renewable energy source must be employed. However, the origin of hydrogen can be diverse: from the traditional reforming processes to others that are environmentally friendly (free of $CO_2$), such as electrolysis [24] or biomass gasification [25]. On the other hand, $N_2$ could be produced by electrochemical separation processes with high efficiency [26] or by conventional separation processes from the air.

On the other hand, there are various review papers focusing on the production of green ammonia to decarbonize the current fossil-fuel based ammonia industry [18,20,21,27]. Green ammonia production can be carried out through ammonia electrosynthesis [20,27,28]. This method consists in an electrochemical process, where nitrogen is fed to the cathode and hydrogen to the anode in proton conducting cells. The reactions taking place are:

$$N_2 + 6H^+ + 6\ e^- \leftrightarrow 2\ NH_3 \quad (1)$$

$$3H_2 \leftrightarrow 6H^+ + 6\ e^- \quad (2)$$

Electrosynthesis of ammonia consumes about 20% lower energy than the Haber-Bosch and it is carried out at low temperature and pressure conditions. However, this technology presents a low selectivity and poor maturity.

In recent years, the generalized interest in hydrogen production from ammonia has made it a target in research as revealed by the increasing number of publications in this topic (Figure 2, from Scopus).

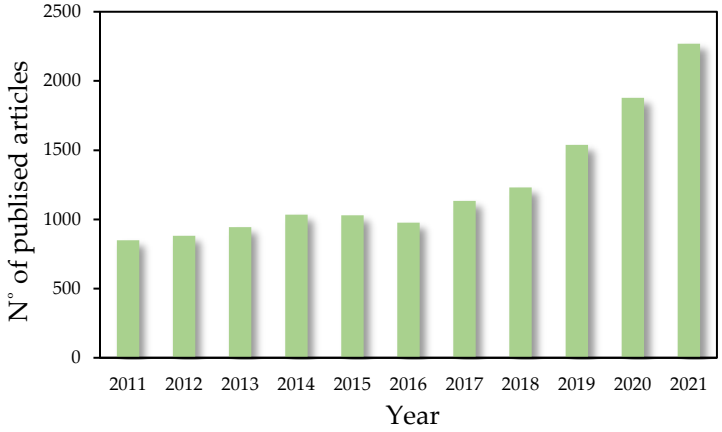


**Figure 2.** Trend of published articles on the topic of 'hydrogen from ammonia' in the last 10 years (source Scopus: 17 September 2022)

Hydrogen can be produced from ammonia by various technologies, such as thermal decomposition, microwave, plasma technologies, solar energy and/or ammonia electrolysis [17]. Among them, the catalytic thermal decomposition of ammonia is the most usual technology for the hydrogen production, owing to the maturity, it can be carried out with or without catalysts and coupled with other parallel exothermic reactions [14].

The key challenges of $NH_3$ as a carrier of $H_2$ are both the decomposition of ammonia and the separation of $H_2$ of the reaction products. These processes must be energy efficient, reliable and scalable to enhance the ammonia perspective as hydrogen carrier toward the 'hydrogen economy' while achieve fulfilling the requirements of a decarbonized economy, in line with the EU energy policy [29,30].

## 3. Catalytic thermal decomposition of $NH_3$

Ammonia decomposition by using heterogeneous catalysts is greatly interesting because it allows the release of $H_2$ in a catalytic reactor. The resulting $H_2$ can be used in-situ, either in fuel cells or by direct combustion. Furthermore, this reaction yields $H_2$ and $N_2$ as byproduct without carbon ($CO_x$) emissions. The hydrogen purification can be easily carried out in $H_2$-permeable membrane reactors [22]. In this sense, some of the current problems associated with the 'hydrogen economy' are avoided, such as its storage and distribution, taking advantage of the benefits related to the use of ammonia.

Most of the investigations that aim to generate $H_2$ from $NH_3$ decomposition are performed at elevated temperatures [14,15,31]. However, the application of $NH_3$ as a hydrogen carrier requires in-situ production at suitable reaction conditions (temperatures and pressures) to be used in fuel cells. Therefore, one of the current main challenges is the development of a sufficiently active catalytic system at low temperatures with an affordable cost.

The ammonia decomposition reaction ($NH_3 \leftrightharpoons \frac{3}{2} H_2 + \frac{1}{2} N_2 \ \Delta H^0 = +46 \text{ kJ mol}^{-1}$) is slightly endothermic, whose kinetics depends on two factors: ammonia concentration in the feed and temperature [14]. Currently, a lot of works have been carried out using different active phases and supports to identify the ammonia decomposition mechanism [14,32–34], although the most accepted one includes six steps as suggested by Temkin [14]. It begins with the ammonia adsorption in the active sites of the catalyst. Then, the adsorbed $NH_3$ molecules undergo consecutive N-H bond breaks, releasing hydrogen atoms that combine to form $H_2$. The final step involves the desorption and recombination of nitrogen atoms to produce $N_2$. This mechanism has been reported to follow these six consecutive steps:

Step 1: $NH_3(g) \leftrightarrows NH_3(a)$ (1)

Step 2: $NH_3(a) + s \leftrightarrows NH_2(a) + H(a)$ (2)

Step 3: $NH_2(a) + s \leftrightarrows NH(a)+H(a)$ (3)

Step 4: $NH(a) + s \leftrightarrows N(a)+H(a)$ (4)

Step 5: $2H(a) \leftrightarrows H_2(g)+2s$ (5)

Step 6: $2N(a) \rightarrow N_2(g)+2s$ (6)

where s symbolizes a vacant site of the catalysts surface, (g) denotes for gas and (a) indicates for adsorbed molecules. However, two phenomena behave as limiting stages of the reaction regardless of the catalysts: the desorption of nitrogen and the breaking of the N-H bond, and both steps are influenced by the chemical properties of the active metal surface (composition and morphology) as well as the support [14,35].

In the high temperature (between 520-690 °C) and high ammonia concentration (50-780 torr) the ammonia reaction is first order concerning ammonia concentration [36]. In the case of working at low temperatures (<400 °C) and high partial pressures of ammonia, it was observed a zero order dependence of the reaction rate on ammonia [14]. Nevertheless, in the high temperature range, both at low ammonia pressure values and feeding it pure, the inhibition by hydrogen did not appear to be significant [36].

Therefore, in any case, the N-M bond strengths (i.e. M= active metal surface) is the key in the design of catalysts for ammonia decomposition reaction, and it should be strong for the N-H bond scission (or $NH_x$ dehydrogenation steps) to take place but adequately weak to desorb $N_2$ [32].

*Ganley et al.* [35] correlated the reaction rate of ammonia decomposition for different metals and the relative rate of N-H bond scission and N-N recombination (estimated from Blowers-Masel correlation). These authors suggested that the rate-limiting for ruthenium (Ru), nickel (Ni), cobalt (Co), iron (Fe) and chromium (Cr) catalysts was nitrogen desorption, whereas for rhodium (Rh), iridium (Ir), platinum (Pt), palladium (Pd) and copper (Cu) the limiting step changed showing a large effect of the active metal surface.

On the other hand, *Boisen et al.* [37] studied different metals for both the synthesis and decomposition of ammonia, mainly focused on the rational design of catalysts for the latter one. Figure 3 shows the volcano-type correlation between ammonia decomposition rate and nitrogen binding energy. They found that nitrogen binding energies were lower on Ru and Ni with high $NH_3$:$H_2$ ratio, whereas with low $NH_3$:$H_2$ ratio the nitrogen binding energies were stronger, which indicated that the optimal catalysts for ammonia synthesis did not work for its decomposition.

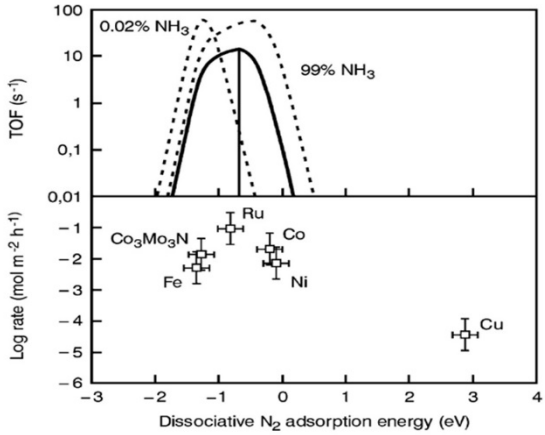


**Figure 3**. Calculated turnover frequencies of ammonia synthesis/decomposition at 773 K, 1 bar, 3:1 $H_2/N_2$, and 0.02, 20 (solid line), and 99% $NH_3$ as a function of the reaction energy of dissociative $N_2$ adsorption. The vertical line gives the dissociative nitrogen binding energy of the optimal ammonia decomposition catalyst when the ammonia concentration is 20%. At these conditions the gas phase equilibrium $NH_3$ concentration is 0.13% (top). Experimental rates of ammonia decomposition over various catalysts at 773 K, 1bar, 3:1 $H_2/N_2$, and 20% $NH_3$ (bottom). Reprinted with permission from [37]. Copyright 2005, Elsevier.

Both studies are considered an essential reference on the design of catalysts based on the rate-determining step for ammonia decomposition. However, there is not a general assumption for the rate-determining step and each catalytic system requires to be examined in detail [14,34]. Despite this, these studies concluded that Ru is the most active metal phase for the ammonia decomposition reaction.

On the other hand, *Lucentini et al*. [14] compared the global warming power on a 100-year basis (kg $CO_2$ $kg^{-1}$) of the elements versus the price of the active metal phase (USD $kg^{-1}$). As shown in Figure 4 Ru must be avoided due to the high environmental impact related to the use of this element. For that reason, an alternative to Ru is the application of cheaper metals in catalytic supports that enhance ammonia decomposition, also using suitable precursors and optimal operating conditions.

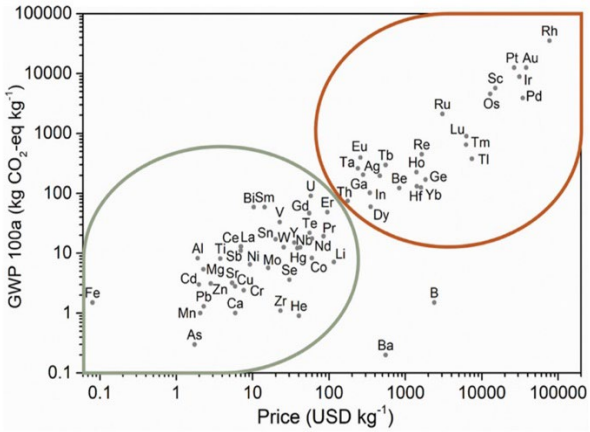


**Figure 4**. Comparison of the price (USD $kg^{-1}$) and the global warming power on a 100-year basis (kg $CO_2$ $kg^{-1}$) of the elements. Reprinted with permission from [37]. Copyright 2005, ACS.

Apart from all the above, the structure of the catalysts and the configuration of the active site have an important effect on anchoring the ammonia molecule, as well as the existence of vacant sites, to release nitrogen and hydrogen atoms. In fact, the metal crystallite size is essential for the catalytic activity since it is a structure-sensitive reaction [38–46]. Overall, a small metal crystallite size leads to a high ammonia conversion, and hence, a higher hydrogen production.

Ru active sites are made up of crystallite size around 3-5 nm and they are called B5-type sites. This involves one layer of three Ru atoms and two further atoms in the layer directly above [38]. In addition, the shape of the nanoparticles plays a significant role in the generation of theses active sites. Indeed, the optimal catalytic activity was found for crystallite of elongated shape of 7 nm, whereas for crystallite of hemispherical particle shape of 2-5 nm [39]. The B5-type sites presented a suitable N-M bond strength improving the reaction mechanism.

In the case of non-noble metals, crystallite sizes between 2-15 nm maximizing the ammonia conversion at low temperatures [45,46]. In particular, nickel size in the range 3 to 5 nm decreased the energy barrier achieving an excellent hydrogen production due to the presence of active sites of B5-type [45]. Moreover, first-principles calculations have concluded that the desorption of N took place more easily on Ni(111) [47]. For Co catalysts, *Bell et al.* [46] suggested that the ammonia conversion was enhanced as the cobalt size diminished, obtaining the maximum activity at 10-20 nm [48].

Considering the promoters, the use of alkaline, alkaline-earth, and rare-earth precursors are reported to enhance the catalytic activity due to an increase in the surface area, a reduction in the pore volume and an increase of the electron density of the metals by rising

the basicity of the catalysts. In addition, it is known that the promoters could decrease the metal size and enhance the stability of the catalyst by hindering the metal agglomeration [42,49–51].

In particular, the use of lanthanum (La) as a promoter results in not only morphological changes of Ni and/or Co actives sites but also electronics effects, facilizing recombinant nitrogen desorption and hence increasing the reaction rate. Furthermore, the studies show that the use of small amounts of cerium (Ce) greatly reduces the decomposition temperature of ammonia. *Zheng et al.* [52] estimated an optimum molar ratio Ce/Ni that allowed to control the crystallite size of Ni, inhibiting their growth.

The support has a key role in the design of catalysts since it influences their properties. They are used to enhance the size, shape and dispersion of the active phase, likewise it might affect the electronic structure of the metals [53]. Actually, a high electron conductivity, basicity, thermal stability and the absence of electron-withdrawing species are the best requirements for a suitable catalytic support for this reaction [14,48,53]. These properties benefits the electrons transfer from the support to the metals, accelerating the desorption of N [32]. In spite of the supports with a high surface area allow to generate highly dispersed metal with small particle sizes [14], recently, materials with a low surface area, such as silicon carbide (SiC) or perovskite-derived catalysts, have shown an excellent performance in the hydrogen production from ammonia [40,42–44,54].

In light with this, this review summarized and compared recent advances in novel, economic and active catalysts for this reaction, paying particular attention to materials with a low surface area (< 35 $m^2$ $g^{-1}$) such as silicon carbide or perovskites ($ABO_3$ structure). The effect of the supports, the active metal and the addition of promoters have been analyzed in detail in these non-porous materials.

## 4. Recent insights into low surface area catalysts for catalytic thermal decomposition of $NH_3$

Ruthenium catalysts supported on low surface area materials have been widely studied in the literature. These showed the highest catalytic activity at low temperatures. Among the support properties, basicity and conductivity have an important role to enhance the ammonia conversion despite the intrinsic low porosity as occurred for rare-earth oxide supports or SiC.

On the one hand, non-noble metals have been also tested in the decomposition of ammonia. Among these, nickel and cobalt are the most studied as active phase of low surface area catalysts. The synthesis method or the utilization of precursors, such as perovskites, are key to the generation of a small metal size. Moreover, the addition of promoters improves the activity at low temperatures.

The use of a bimetallic phase or combination of metals are looking into as a promising alternative in the case of a low surface area catalyst. In particular, the $Co_3Mo_3N$ material presents small porosity and high activity.

The different catalysts available in the literature for the $NH_3$ decomposition that have been recently published, are classified according to their active phase in Table 1-2. Note that, the catalytic activity was evaluated at atmospheric pressure and based on the gas composition feed. However, other experimental factors (support, promoters, gas hourly space velocity, etc.) clearly have an impact on the ammonia conversion. It is important to note that activity decreases with the increase of the gas hourly space velocity and with the increase of the $NH_3$ inlet flow [14].

### 4.1 Ruthenium based catalysts

#### 4.1.1 Novel silicon carbide support

As above mentioned, Ru catalysts exhibit excellent catalytic activity. In this sense, our research group have recently investigated for the first time the use of Ru supported on SiC as a catalysts for ammonia decomposition reaction [40]. Despite of SiC presented a

low specific surface area (25 $m^2$ $g^{-1}$), this ceramic material presents interesting properties (i.e., high resistance, chemical inertness, mechanical strength, high thermostability and conductivity). In light with this, a series of Ru/SiC catalysts were synthesized by vacuum impregnation method with different metal loadings (1-5 wt.% of metal). In addition, the influence of the calcination conditions ($N_2$ or air flow, static air or non-calcined) as well as the reduction temperature (400 °C and 600 °C) were optimized. A maximum catalytic activity (ammonia conversion close to 100% at 350 °C) was obtained at 60000 mL-$NH_3$/Ar $g_{cat}^{-1}$ $h^{-1}$ for the catalyst containing 2.5 wt.% Ru, calcined in a $N_2$ atmosphere and reduced at 400 °C. The authors attributed this behavior to the higher proportion of chlorine species (Cl derived from the Ru precursor) removed during the calcination process and the smallest sizes of Ru (5 nm) generated at lower reduction temperatures. Additionally, the material demonstrated long-term stability after 24 h of reaction. This work corroborated that a low surface area material such as SiC was a suitable support for the nanosized Ru catalysts, allowing to operate at one of the lowest reaction temperature for hydrogen production from ammonia decomposition in this field [55].

#### 4.1.2 Rare-earth oxides supports

On the other hand, other supports based on rare-earth oxides, especially ceria ($CeO_2$) and lanthanum oxide ($La_2O_3$), have been also employed as supports for Ru catalysts [14,56–60]. These metal oxides are conventional supports characterized by a low cost, high basicity, and a great capacity to produce strong metal-support interactions that protected against metal sintering, due to the oxygen vacancies of the materials. However, these metal oxides do not show high surface area values (around 10-20 $m^2$ $g^{-1}$).

*Hu et al.* [56] discovered that Ru (7 wt.%) supported on $CeO_2$ (nanorods) showed a catalytic activity over 8 times higher than Ru supported on carbon nanotubes (CNT) counterpart system, the most active catalysts in the state-of-art literature when feeding pure ammonia. The strong metal-support interactions as well as the generation of small particles (~3 nm) on the Ru/$CeO_2$ caused an improvement of the ammonia conversion. Additionally, the utilization of sodium (Na) as promoter reduced the metal size and enhanced the electronic state of Ru, increasing the ammonia conversion at low temperatures. Meanwhile, *Furusawa et al.* [57] prepared a chlorine-free Ru/$CeO_2$ catalyst (5 wt.%) by incipient wetness impregnation and subsequent washing with 0.01 M of aqueous ammonia. Moreover, the influence of promoter/Ru molar ratio was adjusted together with the reduction conditions (with or without $H_2$ pretreatment). The addition of promoter, cesium (Cs), improved the catalytic activity because of a reduction of the metal particles size (~2 nm), with or without $H_2$ pretreatment, and an increase of the amount of strong basic sites. Therefore, the catalyst with Cs/Ru = 0.43 molar ratio, treated in Ar at 500 °C, resulted in 80% of ammonia conversion at 300 °C at 2000 mL-$NH_3$ $g_{cat}^{-1}$ $h^{-1}$. In both studies, promoters provided an easy desorption of N-adatoms from the surface, which was considered the rate-determining step.

Regarding the use of $La_2O_3$ as support of Ru catalysts, *Huang et al.* [58] reported that the synthesis method of $La_2O_3$ influenced on the hydrogen production from ammonia. They observed that the Ru/$La_2O_3$-700-i (4.8 wt.%) catalyst, prepared by impregnation method, exhibited a 90.7% of ammonia conversion for 84 h at 525 °C and 18000 mL-$NH_3$ $g_{cat}^{-1}$ $h^{-1}$, whereas a 77% was achieved with Ru/$La_2O_3$-700-p (4.8 wt.%) catalyst prepared by a one-step pyrolysis method. The superior activity of the material synthesized by the impregnation method was related to the presence of high pure $La_2O_3$ phase by X-Ray Diffraction (XRD) characterization and the slight variation in the surface area, 20.9 $m^2$ $g^{-1}$ (Ru/$La_2O_3$-700-i) versus 8.0 $m^2$ $g^{-1}$ (Ru/$La_2O_3$-700-p). The addition of potassium hydroxide (KOH) improved the performance of the catalyst.

Considering the utilization of rare-earth oxides as catalytic supports, it is well-known that rare-earth oxides present a small surface area (10-30 $m^2$ $g^{-1}$) although, they are usually employed as catalytic supports for ammonia decomposition [43,44,59,61]. In fact, *Im et al.*

[59] compared the performance of different metal oxides supports and their dependence on the basic properties of Ru catalysts (~2 wt.%). The ammonia conversion at 500 °C and 6000 mL-$NH_3$ $g_{cat}^{-1}$ $h^{-1}$ decreased in order of Ru/ $La_2O_3$ > Ru/$Pr_xO_y$ > Ru/$Sm_2O_3$ ~ Ru/$Gd_2O_3$ > Ru/$Y_2O_3$ > Ru/$Yb_2O_3$ catalysts. It was related to the decrease (in the same order) of the total basic sites and the basic strength of the catalysts. The basic properties influenced the electron state of Ru, enhancing the electron donation from the support to the active phase, and thus, the activity. This was corroborated by $NH_3$-temperature programmed surface reaction ($NH_3$-TPSR) and the promotion of the desorption step of N atoms. Meanwhile, *Zhang et al.* [62] developed a solid milling method, which consisted to mill ruthenium oxide ($RuO_2$) and samarium (III) hydroxide ($Sm(OH)_3$) in a mortar by hand for 10 min, to obtain Ru-$Sm_2O_3$-m (4 wt.%) with a surface area of 28.5 $m^2$ $g^{-1}$. However, it was found that others synthesis methods exhibited a much higher activity due to the greater interaction between Ru and samarium oxide ($Sm_2O_3$) support.

On the other hand, *Le et al.* [63] have recently developed a novel $La_xCe_{1-x}O_y$ composite by the deposition-precipitation method as support of 1.8 wt.% of Ru loading. The optimal catalyst presented a 0.33 and 0.67 molar ratio of La and Ce with a surface area of 31 $m^2$ $g^{-1}$, similar to the rest of the catalysts. However, this material showed a small Ru size with a strong metal-support interaction and the optimized acidity-basicity properties, which enhanced the rate-determining step. This was corroborated by density functional theory (DFT) calculations. Hence, this catalyst achieved 80% of ammonia conversion at 500 °C and 54000 mL-$NH_3$ $g_{cat}^{-1}$ $h^{-1}$.

4.1.3 $ABO_3$ perovskites as Ru supports

In light with the utilization of composites as catalytic supports, a series of $ABO_3$ perovskite materials, $Sr_{1-x}Y_xTi_{1-y}Ru_yO_{3-\delta}$ (x = 0, 0.08, and 0.16; y = 0, 0.04, 0.07, 0.12, 0.17, and 0.26) were synthesized by a modified Pechini method and tested for ammonia dehydrogenation, whose surface area varied from 25 to 40 $m^2$ $g^{-1}$ [64]. The influence of A or B site substitution on the catalytic ammonia dehydrogenation activity was determined by varying the quantity of either A or B site cation. The authors suggested that the simultaneous formation of $SrRuO_3$ and $Ru^0$ generated suitable interactions, although they did not give any information about this. However, ammonia decomposition was improved and the $Sr_{0.84}Y_{0.16}Ti_{0.92}Ru_{0.08}O_{3-\delta}$ (8 mol % of Ru) displayed 96% of conversion at 500 °C and 10000 mL-$NH_3$ $g_{cat}^{-1}$ $h^{-1}$ for long-reaction times. More recently, $La_{1-x}Sr_xAlO_3$ typical perovskite-oxide, prepared by citrate sol-gel method, was reported to be an efficient support, with small surface area (~18 $m^2$ $g^{-1}$), for Ru (3 wt.%) catalysts [65]. The properties of the supports were modulated and adjusted by tailoring the cation substitution of $La^{3+}$ by $Sr^{3+}$ and it was discovered that the activity strongly depended on the nature of $La_{1-x}Sr_xAlO_3$. In particular, characterization results of Ru/$La_{0.8}Sr_{0.2}AlO_3$ showed the highest electro-rich state of metallic Ru, which promoted the reaction mechanism.

Additionally, *Zhiqiang et al*. [66] have employed different alkali metal silicates $A_2SiO_3$ (A = Li, Na and K) as supports prepared by a sol-gel method. The formation of silicate structure resulted in a reduction in the surface area (< 10 $m^2$ $g^{-1}$). The $K_2SiO_3$ material, with the lowest surface area (3.2 $m^2$ $g^{-1}$), exhibited the highest catalytic activity (60.5% of $NH_3$ conversion at 450 °C and 30000 mL-$NH_3$ $g_{cat}^{-1}$ $h^{-1}$). The maximum performance was caused by an increase of the strength and number of basic sites and suitable metal-support interactions, which were related with the highest content of oxygen vacancies. In addition, these properties led to small Ru particles size.

4.1.4 Metal oxides supports

Based on layered double hydroxides (LDHs), recently *Zhao et al.* [67] have employed calcium (Ca)-alumina (Al)-LDHs with low surface area for ammonia decomposition. The LDHs allowed to synthesize nanoparticles with designed morphological and structural characteristics despite of their relatively inert oxides. The influence of the synthesis method on ammonia decomposition was studied. Firstly, an aqueous solution of Ru

(Ru/$CaAlO_x$-w), and secondly, an ethanol solution of Ru was incorporated by impregnation (Ru/$CaAlO_x$-e). Thus, spherical or elliptical Ru particles were embedded with the $CaAlO_x$ with strong metal-support interactions when water was utilized, while spots of big diameter were obtained with ethanol. In this sense, the spherical or elliptical Ru particles and the higher metal-support interaction enhanced the reaction at low temperatures.

Another very interesting metal oxide of a low surface area (~30 $m^2\ g^{-1}$) employed as support of Ru was zirconia ($ZrO_2$). This material is an amphoteric supports because it acts as base or an acid, i.e., it is capable of donating and accepting protons, and hence, it could not be considered an ideal support for the hydrogen generation from ammonia decomposition [34]. However, the characteristics of this material can be easily altered by chemical or physical routes [68].

In this sense, different barium doped-zirconia (Ba-$ZrO_2$) supports were compared as support of 3 wt.% of Ru catalysts [68]. It was found that the material synthesized by sol-gel process (Ru/Ba-$ZrO_2$) in comparison with the support prepared by conventional immersion (Ru-Ba/$ZrO_2$) demonstrated a higher activity in the $NH_3$ decomposition reaction. The superior ammonia conversion of Ru/Ba-$ZrO_2$ (100% at 450 °C and 3000 mL-$NH_3$ $g_{cat}^{-1}$ $h^{-1}$) versus that of Ru-Ba/$ZrO_2$ (10% at the same conditions) was a consequence of the formation of $BaZrO_3$ phase, which improved the electron-transfer from the support to Ru, and hence, accelerating the rate-determining step of the reaction.

In other work, *Hu et al.* [69] reported a novel metal-organic framework (MOF) prepared from a zirconia precursor, leading to a mesoporous crystalline zirconia (MPC- $ZrO_2$) of low area (2 $m^2\ g^{-1}$). They studied the influence of Ru loading (0.8-6.5 wt.%) as well as the Cs loading (2.5-10 wt.%). The synthesis of Ru catalysts by incipient wetness impregnation method allowed to obtain small Ru nanoparticles (~3 nm) confined within the rigid crystalline MPC- $ZrO_2$ with strong metal-support interactions. As expected, the $NH_3$ conversion increased with the Ru loading until a maximum value was obtained for 5 wt.% of Ru, as shown in Table 1. Moreover, 5 wt.% of Cs was selected as the optimal Cs loading, because a further increase decreased the activity, may be due to the blockage of the active sites. On the other hand, the basic properties of zirconia were controlled by doping with La and alkaline earth metals, using a coprecipitation method while Ru (0.5 wt.%) was incorporated by wet impregnation [70]. The addition of La and strontium (Sr) increased weak, medium, and strong basic sites, whereas magnesium (Mg) and Ca only improved weak and medium basic sites.

On the other hand, the most used support in this reaction was alumina oxide ($Al_2O_3$), nonetheless, it generally showed a large surface area [14,34]. To the best of our knowledge, only one recent manuscript described a Ru catalyst supported on $Al_2O_3$ doped with La (10Ru-La(50)- $Al_2O_3$) with a low surface area (23.3 $m^2\ g^{-1}$) [71]. The authors suggested that a newly phase $LaAlO_3$ formed during the synthesis method strongly interacted with Ru active sites, facilitating ammonia dehydrogenation even at low temperatures. This material achieved an ammonia conversion of 68.9% at 400 °C and 2300 mL-$NH_3$ $g_{cat}^{-1}$ $h^{-1}$.

Taking into account the utilization of alkaline earth metal oxides with low surface area as supported Ru catalysts, the magnesia (MgO) and calcium oxide (CaO) were reported [72]. The work carried out by *Sayas et al*. [72] optimized Ru/CaO catalysts promoted with potassium (5-15 wt.%) to perform ammonia decomposition reaction at high pressure. Commercial CaO and MgO presented small surface area (values between 4-30 $m^2\ g^{-1}$) and Ru (1-7 wt.%) was incorporated by incipient wetness impregnation. In spite of the specific area, CaO showed a large number and stronger basic sites, and it allowed to generate an average Ru nanoparticle size of 6 nm. The reaction was also performed at atmospheric pressure and the catalysts were optimized. The maximum activity (61.0% of conversion at 400 °C and 9000 mL-$NH_3$ $g_{cat}^{-1}$ $h^{-1}$) was achieved with 3 wt.% and 10 wt.% of Ru and K loadings, respectively, which was a consequence of the suitable Ru nanoparticle size.

**Table 1**. Catalytic activity of Ruthenium based catalysts for $H_2$ production from $NH_3$ decomposition performance at 1 atm.

| Catalysts | Ru loading (wt.%) | $S_{BET}$ ($m^2\ g^{-1}$) | GHSV ($mL \cdot g_{cat}^{-1} \cdot h^{-1}$) | $NH_3$ inlet flow (%) | T (°C) | $NH_3$ conversion (%) | $H_2$ formation rate (mmol $H_2\ g_{cat}^{-1}\ min^{-1}$) | Ref. |
|---|---|---|---|---|---|---|---|---|
| 2.5Ru/SiC-600-$N_2$ flow | 2.5 | 25.9 | 60000 | 5 | 350 | 80.2 | 2.53 | [40] |
| 2.5Ru/SiC-600- air flow | 2.5 | 26.9 | 60000 | 5 | 350 | 72.3 | 2.37 | |
| 2.5Ru/SiC-600-static air | 2.5 | 25.6 | 60000 | 5 | 350 | 67.5 | 2.06 | |
| 2.5Ru/SiC-600-non-calcined | 2.5 | 29.3 | 60000 | 5 | 350 | 69.8 | 2.17 | |
| 1Ru/SiC-400-$N_2$ flow | 1.0 | 28.8 | 60000 | 5 | 350 | 59.6 | 2.00 | |
| 2.5Ru/SiC-400-$N_2$ flow | 2.5 | 26.3 | 60000 | 5 | 350 | 98.7 | 3.30 | |
| 5Ru/SiC-400-$N_2$ flow | 5.0 | 25.5 | 60000 | 5 | 350 | 86.6 | 2.90 | |
| 1Ru/SiC-600-$N_2$ flow | 1.0 | 28.8 | 60000 | 5 | 350 | 41.5 | 1.31 | |
| 5Ru/SiC-600-$N_2$ flow | 5.0 | 25.5 | 60000 | 5 | 350 | 89.9 | 2.91 | |
| Ru/$CeO_2$-NR | 7.0 | 15.0 | 6000 | 29 | 350 | 23.0 | 1.54 | [56] |
| Ru-Na/$CeO_2$-NR | 7.0 | 10.0 | 6000 | 29 | 350 | 25.0 | 1.67 | |
| Ru/$CeO_2$ | 5.0 | 14.6 | 2000 | 100 | 350 | 60.0 | 26.80 | [57] |
| Ru-Cs/$CeO_2$ | 5.0 | 13.1 | 2000 | 100 | 350 | 98.0 | 44.00 | |
| Ru/$La_2O_3$-700-i | 4.8 | 20.9 | 18000 | 100 | 400 | 40.0 | 8.04 | [58] |
| Ru/$La_2O_3$-700-p | 4.8 | 8.0 | 18000 | 100 | 400 | 35.0 | 5.02 | |
| Ru/$La_2O_3$-700-i-K | 4.8 | - | 18000 | 100 | 400 | 50.0 | 10.04 | |
| Ru/$Y_2O_3$ | 2.0 | 29.2 | 6000 | 100 | 500 | 82.6 | 5.53 | [59] |
| Ru/$La_2O_3$ | 2.1 | 22.2 | 6000 | 100 | 500 | 95.6 | 6.40 | |
| Ru/$Pr_xO_y$ | 2.0 | 15.3 | 6000 | 100 | 500 | 93.0 | 6.23 | |
| Ru/$Sm_2O_3$ | 2.1 | 9.4 | 6000 | 100 | 500 | 85.6 | 5.73 | |
| Ru/$Gd_2O_3$ | 2.0 | 11.6 | 6000 | 100 | 500 | 85.2 | 5.71 | |
| Ru/$Yb_2O_3$ | 1.9 | 25.6 | 6000 | 100 | 500 | 28.6 | 1.92 | |
| 4Ru/$Sm_2O_3$-m | 3.5 | 28.5 | 30000 | 100 | 450 | 15.7 | 4.90 | [62] |

**Table 1**. Continued.

| Catalysts | Ru loading (wt.%) | $S_{BET}$ ($m^2$ $g^{-1}$) | GHSV ($mL \cdot g_{cat}^{-1} \cdot h^{-1}$) | $NH_3$ inlet flow (%) | T (°C) | $NH_3$ conversion (%) | $H_2$ formation rate (mmol $H_2$ $g_{cat}^{-1}$ $min^{-1}$) | Ref. |
|---|---|---|---|---|---|---|---|---|
| $Ru/La_{0.33}Ce_{0.67}$ | 1.8 | 31.0 | 6000 | 100 | 400 | 93.0 | 6.23 | [63] |
| $Ru/La_{0.5}Ce_{0.5}$ | 1.8 | 28.0 | 6000 | 100 | 400 | 86.0 | 5.76 | |
| Ru/La | 1.8 | 30.0 | 6000 | 100 | 400 | 41.0 | 2.75 | |
| $Sr_{0.92}Y_{0.08}Ti_{0.88}Ru_{0.12}O_{3-\delta}$ | 6,1 mol % | 33.5 | 10000 | 100 | 350 | 2.3 | 0.25 | [64] |
| $Sr_{0.92}Y_{0.08}Ti_{0.74}Ru_{0.26}O_{3-\delta}$ | 12,4 mol % | 24.5 | 10000 | 100 | 350 | 18.4 | 2.05 | |
| $Sr_1Y0Ti_{0.91}Ru_{0.09}O_{3-\delta}$ | 4,22 mol % | 31.1 | 10000 | 100 | 350 | 3.2 | 0.36 | |
| $Ru/LaAlO_3$ | 3 | 18.1 | 30000 | 100 | 500 | 50.0 | 75.00 | [65] |
| $Ru/La_{0.9}Sr_{0.1}AlO_3$ | 3 | 18.4 | 30000 | 100 | 500 | 60.0 | 90.00 | |
| $Ru/La_{0.8}Sr_{0.2}AlO_3$ | 3 | 18.8 | 30000 | 100 | 500 | 71.6 | 107.40 | |
| $Ru/La_{0.7}Sr_{0.3}AlO_3$ | 3 | 18.5 | 30000 | 100 | 500 | 55.7 | 83.55 | |
| $Ru/Li_2SiO_3$ | 3.4 | 8.5 | 30000 | 100 | 450 | 30.0 | 10.4 | [66] |
| $Ru/Na_2SiO_3$ | 3.5 | 9.6 | 30000 | 100 | 450 | 52.0 | 17.8 | |
| $Ru/K_2SiO_3$ | 3.2 | 3.6 | 30000 | 100 | 450 | 60.5 | 20.3 | |
| Ru/CaAlOx-e | 3.5 | 11.3 | 6000 | 100 | 400 | 8.5 | 0.57 | [67] |
| Ru/CaAlOx-w | 3.5 | 11.8 | 6000 | 100 | 400 | 38.0 | 2.54 | |
| $Ru/ZrO_2$ | 3.0 | 38.6 | 3000 | 100 | 500 | 20.0 | 1.34 | [68] |
| $Ru/Ba\text{-}ZrO_2$ | 3.0 | 25.4 | 3000 | 100 | 500 | 100.0 | 3.35 | |
| $Ru\text{-}Ba/ZrO_2$ | 3.0 | 6.3 | 3000 | 100 | 500 | 10.0 | 0.67 | |
| $0.8Ru/MPC\text{-}ZrO_2$ | 0.8 | 8.0 | 6000 | 29 | 350 | 0.0 | 0.00 | [69] |
| $2Ru/MPC\text{-}ZrO_2$ | 2.0 | 20.0 | 6000 | 29 | 350 | 1.1 | 0.07 | |
| $3.5Ru/MPC\text{-}ZrO_2$ | 3.5 | 18.0 | 6000 | 29 | 350 | 3.9 | 0.26 | |
| $5Ru/MPC\text{-}ZrO_2$ | 5.0 | 12.0 | 6000 | 29 | 350 | 6.5 | 1.59 | |
| $6.5Ru/MPC\text{-}ZrO_2$ | 6.5 | 10.0 | 6000 | 29 | 350 | 2.1 | 0.14 | |
| $5Ru2.5Cs/MPC\text{-}ZrO_2$ | 5.0 | 11.0 | 6000 | 29 | 350 | 4.1 | 0.27 | |

**Table 1**. Continued.

| Catalysts | Ru loading (wt.%) | $S_{BET}$ ($m^2$ $g^{-1}$) | GHSV ($mL \cdot g_{cat}^{-1} \cdot h^{-1}$) | $NH_3$ inlet flow (%) | T (°C) | $NH_3$ conversion (%) | $H_2$ formation rate (mmol $H_2$ $g_{cat}^{-1}$ $min^{-1}$) | Ref. |
|---|---|---|---|---|---|---|---|---|
| 5Ru5Cs/MPC-$ZrO_2$ | 5.0 | 7.5 | 6000 | 29 | 350 | 19.4 | 4.47 | [69] |
| 5Ru10Cs/MPC-$ZrO_2$ | 5.0 | 3.0 | 6000 | 29 | 350 | 5.8 | 0.39 | |
| Ru/$ZrO_2$ | 0.5 | 28.0 | 4600 | 100 | 400 | 60.4 | 5.13 | [70] |
| Ru/$ZrO_2$ | 2.0 | 4.9 | 6000 | 100 | 500 | 0 | 0 | [59] |
| Ru/La(50)-$Al_2O_3$ or $LaAlO_3$ | 0.7 | 23.3 | 2300 | 10 | 400 | 68.5 | 1.76 | [71] |
| 5Ru10K/MgO | 4.8 | 32.0 | 9000 | 100 | 400 | 39.4 | 3.96 | [54] |
| 1Ru10K/CaO | 0.9 | 6.0 | 9000 | 100 | 400 | 8.5 | 0.85 | |
| 2Ru10K/CaO | 1.8 | 7.0 | 9000 | 100 | 400 | 40.0 | 4.02 | |
| 3Ru10K/CaO | 2.8 | 5.0 | 9000 | 100 | 400 | 61.0 | 6.13 | |
| 5Ru10K/CaO | 4.7 | 4.0 | 9000 | 100 | 400 | 53.7 | 5.39 | |
| 7Ru10K/CaO | 6.6 | 8.0 | 9000 | 100 | 400 | 35.0 | 3.52 | |
| 3Ru/CaO | 2.9 | 10.0 | 9000 | 100 | 400 | 5.0 | 0.50 | |
| 3Ru5K/CaO | 2.8 | 5.0 | 9000 | 100 | 400 | 20.0 | 2.01 | |
| 3Ru15K/CaO | 2.7 | 5.0 | 9000 | 100 | 400 | 60.0 | 6.03 | |

4.2 Non-noble metals based catalysts

In order to avoid the utilization of ruthenium as the active phase because of its high price and environmental impact, as mentioned in Section 2, other non-noble metals e.g., (Ni, Co, Fe, Cu, molybdenum (Mo), etc.) should be considered for the design of heterogeneous catalysts for ammonia decomposition reaction. Note also that, although these materials did not exhibit an activity as high as that of Ru, they are economically viable and ecofriendly [14,34,55].

4.2.1 Novel silicon carbide support

Based on the excellent properties delivered by novel SiC as support for Ru catalysts, *Pinzon et al*. [42] also synthesized, for the first time, Co (5 wt.%) supported on SiC. Additionally, different promoters (alkaline, alkaline earth and rare-earth metals) have been studied and optimized. The addition of certain promoters could reduce the reaction temperature in Co/SiC catalysts. It was found that the addition of 1 wt.% of K and La improved the ammonia conversion whereas the addition of other promoters did not enhance (Cs and Ce) or even decreased (Mg and Ca) the activity with respect to the unpromoted catalyst. For instance, Cs did not increase the basic sites and Ce could be inhibited by hydrogen. Regarding Mg and Ca, the metal dispersion was lower. The basicity and electron-donor properties of Co catalysts were improved by an optimized K amount of 1 wt.%, which enhanced the activity with respect to La. Nonetheless an increase of the K loading led to the blockage of the active sites. Thus, Co-1K/SiC resulted to be an excellent and stable catalyst providing a conversion close to 100 % at 450 °C and 60000 mL-$NH_3$-Ar $g_{cat}^{-1}$ $h^{-1}$ for one day of reaction.

4.2.2 Rare-earth oxides supports

Other less novel supports of low surface area are based on metal oxides, mainly rare-earth oxides ($La_2O_3$, $CeO_2$, $Y_2O_3$, $Sm_2O_3$ and $Gd_2O_3$). These have been widely employed as supports of cobalt and nickel catalysts [73–77]. In fact, for the first time *Okura et al*. [75] prepared a screening of Ni (10 wt.%) catalysts supported on rare-earth oxides by conventional impregnation method and probed on the ammonia decomposition reaction. These materials showed a small surface area (< 10 $m^2$ $g^{-1}$) with an adequate activity on this reaction as a consequence of the low effect of hydrogen inhibition. In particular, Ni/$Y_2O_3$ exhibited the best catalytic activity owing to the lowest amount of strongly adsorbed hydrogen. In other work, the influence of alkaline earth metals (Mg, Ca, Sr and Ba) over Ni/$Y_2O_3$ catalyst on the reaction was also studied by the same group [73]. It was found that Sr and Ba enhanced the activity of Ni catalysts since alkaline earth metals interacted strongly with Ni. This interaction improved the basic properties favoring the desorption of nitrogen atoms (rate-determining step) and accelerating the reaction mechanism at low temperatures.

Other authors investigated the influence of synthesis conditions on Ni [74] and Co [76] supported on $La_2O_3$ as well as the influence of the MgO as promoter. First, the calcination temperature of lanthanum oxide affected the catalytic activity of Ni as follows: 10Ni/$La_2O_3$-450 > 10Ni/$La_2O_3$-550 > 10Ni/$La_2O_3$-650 ~ 10Ni/$La_2O_3$- 750 ~ 10Ni/$La_2O_3$-850, which was associated with the relative higher specific surface area, higher total basic sites and oxygen species in the surface [74]. In this work, the incorporation of Mg, added by surfactant-templated method, increased the basicity of the catalysts, which improved the Ni electron density enhancing the reaction and yielding 82% of conversion at 550 °C with a nickel loading of 40 wt.%. *Podila et al.* [76] investigated the effect of the calcination atmosphere in Co (5 wt.%) supported on MgO-$La_2O_3$ prepared by co-precipitation from metal nitrates solutions under high super saturation. The material calcined in $N_2$ atmosphere (5CMLa-$N_2$) had higher surface metal concentration and the strongest metal-support interaction, achieving a good catalytic performance. On the other hand, the morphology of ceria also influenced on the activity of cobalt catalysts and the surface area, which

ranged between 20-50 $m^2$ $g^{-1}$ depending of the form of the crystallites [77]. Hence, $CeO_2$-nanocubes showed the lowest area (20 $m^2$ $g^{-1}$) but with the best redox properties, thereby a suitable activity (67% of ammonia conversion at 550 °C).

4.2.3 $ABO_3$ perovskites as supports and catalytic precursors

It is well-known that the rare-earth oxides promote the catalytic effect of nickel and cobalt [14,34,49,75,78]. Nonetheless, they exhibited very small surface area hindering the production of small Ni/Co sizes, which in turn, decrease the activity. Therefore, the benefits of perovskites as catalyst precursors and/or supports were investigated to develop materials with better characteristics than the main metal oxides.

The utilization of perovskite-type oxides ($LaBO_3$) as catalytic precursors of Ni catalysts for ammonia decomposition was firstly carried out by *Muroyama et al.* [79]. These perovskite-type oxides seem like a highly promising precursors in this reaction because the final catalysts (perovskite-derived catalysts) were obtained after the reduction of perovskites under hydrogen flow [43]. That work provided a new insight in the design of diverse, economic, and efficient catalysts to achieve a high activity at low temperature and enhanced the ammonia perspective as a hydrogen carrier toward the 'hydrogen economy', despite of the small surface area (< 30 $m^2$ $g^{-1}$) of these perovskite-derived catalysts.

Recently, *Pinzon et al.* [43] found that the synthesis method (self-combustion), both the fuel to metal nitrates molar ratio and the calcination temperature, was found to play an important role in the properties of the resulting perovskites. In this sense, a citric acid to metal nitrates molar ratio equal to one allowed to generate a $LaNiO_3$ perovskite without impurities and suitable physicochemical properties (higher specific surface area, ~11 $m^2$ $g^{-1}$, and basicity, 17.8 μmol $CO_2$ $g^{-1}$, without impurities, $La_2NiO_4$). Moreover, the calcination temperature affected the size of the final nickel/cobalt catalysts. A calcination temperature of 650 °C led to small and well-dispersed $Ni^0$. For Co perovskites, calcination temperature below 900 °C did not influence on the size of $Co^0$ after reduction. Therefore, Ni and Co perovskite-derived catalysts yielded an excellent ammonia conversion, 98.9% and 97%, respectively, at 450 °C and 75000 mL-$NH_3$-Ar $g_{cat}^{-1}$ $h^{-1}$ with a suitable stability for one day.

Aiming to improve the activity of Ni catalysts derived from perovskite, the addition of different dopant agents could increase the basicity among other properties. Thus, the partial substitution of La cation by Ce [44,80] or by Mg [44] was studied. For that, $La_xA_{1-x}NiO_3$, where A = Ce or Mg and x = 0, 0.1, 0.9 and 1 (molar basis), was synthesized and examined in the hydrogen production from ammonia. It was observed that the addition of the Ce and Mg improved the basicity and the further decrease of the metal size after reduction, which enhanced the catalytic performance. Mainly, a dopant amount of 0.9 molar basis of Ce and Mg led to catalysts with a nickel size of 4.6 nm and 4.1 nm, respectively, whereas 21.2 μmol $CO_2$ $g^{-1}$ and 64.6 μmol $CO_2$ $g^{-1}$, respectively, of total basic sites were obtained. These nickel catalysts yielded a conversion of 96 % ($La_{0.1}Ce_{0.9}NiO_3$) and 98 % ($La_{0.1}Mg_{0.9}NiO_3$) at low temperatures (400 °C) for 40 h of reaction, exhibiting a good stability without deactivation. Mg-doped nickel perovskite was selected as the best dopant of the nickel perovskite, mainly due to the virtuous synergic effect between Ni-Mg-La, which showed a higher basicity and a higher capacity to desorb $N_2$ [44].

The application of perovskite-type oxides as supports of nickel and cobalt catalyst have been proposed by different authors [81,82]. In both studies, the influence of the variation with different alkaline, alkaline earth, and rare-earth of the $ABO_3$ formulation was investigated on th ammonia decomposition, contempt these materials displayed small surface area (< 20 $m^2$ $g^{-1}$) owing to the high calcination temperature (1100 °C) required for their synthesis [82].

On the one hand, $XCeO_3$ (X = Mg, Ca, Sr, Ba) perovskite-type oxides were synthesized by combustion method while cobalt (5 wt.%) was incorporated by wet impregnation [81]. It was found that the activity increased as the electronegativity of the X elements decreased, being the $BaCeO_3$ support the one that presented the highest catalytic activity

because of the highest conductivity, moderate metal-support interaction, and moderate basicity.

On the other hand, *Okura et al*. [82] prepared several formulations of perovskites using the solid-state reaction or the citric acid complex methods. $ANbO_3$ (A = Na and K) and $AETiO_3$ (AE = Ca, Sr, and Ba) were prepared by the first method, while $REAlO_3$ (RE = La, Sm, and Gd), $AEMnO_3$, and $AEZrO_3$ by the latter one. The nickel (40 wt.%) was incorporated by wet impregnation. The supports containing Nb and Mn exhibited a lower conversion at 550 °C, whereas $REAlO_3$, $AETiO_3$ and $AEZrO_3$ supports increased the activity, mainly due to the electronic state of nickel species. Additionally, the $AEZrO_3$ supports exhibited a higher amount of basic sites owing to the smaller electronegativity of Zr. Regarding the electronegativity of the AE elements, Ba and Sr (lower electronegativity in comparison with Ca) increased the number of basic sites, and hence, were responsible of the higher catalytic activity of $Ni/BaZrO_3$ and $Ni/SrZrO_3$. They displayed 93% ($Ni/SrZrO_3$) and 95% ($Ni/BaZrO_3$) of conversion at 550 °C.

4.2.4 Metal oxides supports

Other precursors, based on hydrotalcite materials (derived from layered double hydroxides), allowed to synthesize catalysts with controlled accessibility to the structure, after high temperature reduction [83]. Nickel hydrotalcites based on $Ca^{2+}$ and $Al^{3+}$ cations ($Ni_xCa_2Al_1$-LDHs-ST, x = 0.1, 0.3, 0.5, 1 and 2) were prepared mixing the corresponding nitrates with a $Ca^{2+}/Al^{3+}$ atomic ratio equal to 2, using a precipitating agent (2 M of NaOH, pH = 12). Then, the precipitated was transferred into a Teflon vessel (100 °C for 36 h) and the product was centrifugated, washed and dried overnight. It was found that the gradual incorporation of Ni altered the structure of the $Ca_2Al_1$-LDHs to hydrobobomkulite, and finally, changed into takovite. This transformation led to an increase of the amount of B5-type sites which improved the $NH_3$ decomposition (55% of ammonia conversion at 550 °C and 10000 mL-$NH_3$ $g_{cat}^{-1}$ $h^{-1}$). Despite of the low area of the catalysts (30.1 $m^2$ $g^{-1}$), hydrotalcites seem to be a good precursor for the design of heterogeneous catalysts presenting better catalytic properties than those obtained by the conventional impregnation method ($Ni_1/Ca_2Al_1$-LDHs-IM).

In light with the structure of the supports, fluorite-type oxides with a face-centered-cubic crystal structure (for example, ceria-zirconia alloys, CZY) showed good redox properties, high thermal stability and good capacity to disperse the metals, despite of the small area (values < 30 $m^2$ $g^{-1}$) [84]. Ni, Co and Ni-Co (10 wt.%) catalysts were prepared by incipient wetness impregnation over CZY and tested on ammonia decomposition. Noticeably, the bimetallic catalysts with 9 wt.% of Co and 1 wt.% of Ni ($Ni_1Co_9$/CZY) resulted in the highest activity at 60000 mL-$NH_3$ $g_{cat}^{-1}$ $h^{-1}$ with almost 100% of conversion at 600 °C for 72 h, owing to the formation of a Ni-Co alloy with suitable metals dispersion (20.3%). The authors claimed that the synthesis of these metal oxides (CZY) were an eco-friendly and affordable processes.

Based on an economic, abundant and low surface area material, fresh mica nanosheets ($K_{0.75}Al_2Si_4O_{10}(OH)_2$) have been employed as support of nickel catalysts (20-30 wt.% prepared by wet impregnation) in the reaction [85]. The catalytic activity was improved by the two-dimensional structure of mica since the mass transfer was favored. Other natural nano-structural material, attapulgite (ATP), has been used as support of Ni catalysts (50 wt.% prepared by homogeneous precipitation method) [86]. This synthesis developed materials with a low surface area (< 10 $m^2$ $g^{-1}$) although it showed good performance in the ammonia decomposition, exhibiting a 65% of conversion at 600 °C. The strong metal-support interaction was the responsible of the adequate activity.

*Im et al.* [50] prepared by solid-state reaction different aluminate-based compounds (AM-Al-O, AM = Mg, Ca, Sr and Ba) modified with alkaline earth metals. These were investigated as supports of nickel (20 wt.%) catalysts. Similarly of the above mentioned, the basic properties of the materials changed with the different metals, being the Ni/Sr-

Al-O and Ni/Ba-Al-O catalysts the most basic materials, providing a higher performance in the hydrogen production from ammonia.

4.2.5 Metal imides supports

Recently, the utilization of metal imides ($Mg_3N_2$, CaNH and BaNH) have received attention as support of Co catalysts in the ammonia decomposition reaction. The catalysts were prepared following the procedure described in [87], showing a low surface area. The Co-CaNH material showed the highest specific surface area among the three materials but a lower activity than that of Co-BaNH. The highest activity of Co-BaNH was related to an intermediate phase (Co-N-Ba) which enhanced the energy-efficient reaction pathway.

4.2.6 Others low surface area supports

On the other hand, pure oxides such as $Co_3O_4$ (100Co) [88] or NiO [89,90] have been studied as catalysts in spite of their low area (< 30 $m^2\ g^{-1}$). However, the catalytic activity was low (< 20% of ammonia conversion at 550 °C) at lower temperatures, as can be observed in Table 2, caused by the morphological defects of these materials and their poor stability.

Other monometallic catalysts with small surface area were based on Fe and Mo supported on commercial carbon nanofibers (CF). The materials were prepared by the impregnation method of different metal loadings (4-14 wt.%) providing an area below 40 $m^2\ g^{-1}$ [91]. Mo catalysts displayed lower conversion than Fe catalysts over a conventional heated reaction system. However, the activities of both catalysts improved at lower temperatures in the microwave reaction system, because of the formation of carbide species ($Fe_2C$ and $Mo_2C$), which are found to enhance the transfer of energy to the active phase.

4.3 Bimetallic catalysts metal catalysts

Finally, the utilization of non-noble bimetallic catalysts with low surface area has been also investigated (Table 2). It has been established that the apparent activation energy (Ea) of the bimetallic catalysts was lower than that of the monometallic catalysts, enhancing the ammonia conversion [14].

In this sense, mono and bimetallic perovskites ($LaCo_{1-x}Ni_xO_3$, x = 0, 0.2, 0.4, 0.6, 0.8 and 1 molar basis) were synthesized and tested as catalyst precursors for the ammonia decomposition [44]. However, bimetallic perovskites originated particles size of $Co^0/Ni^0$ (in the range 7.8-5.7 nm) higher than the pure $LaNiO_3$ (4.2 nm) which did not improve the activity. Both impurities and a lower amount of active sites were detected on bimetallic perovskites, which also decreased the ammonia conversion. The higher catalytic activity of nickel perovskite-derived catalysts versus cobalt perovskite-derived catalysts has been corroborated by *Podila et al.* [80].

As illustrated in Section 3, the alloy between Co-Mo is near to the volcano curve, with a suitable N binding energy to easily desorb nitrogen species, being the active phase $Co_3Mo_3N$ [17,92]. *Duan et al.* [92] studied the effect of the calcination atmosphere on metal amine metallate ($Co(en)_3MoO_4$) precursors to obtain an active catalyst based on Co-Mo. They selected argon (Ar) and air (Air) as the calcination atmosphere, which curiously affected the physicochemical properties. Indeed, the textural properties as well as the crystal phase were modified. The CoMo-Ar calcined catalyst showed magnetic properties and a higher surface area (38.5 $m^2\ g^{-1}$) than CoMo-Air (5.7 $m^2\ g^{-1}$). However, in the reduction step the surface area changed, showing 21 $m^2\ g^{-1}$ and 23.7 $m^2\ g^{-1}$ CoMo-Ar and CoMo-Air, respectively, due to the transformation of the crystal phase. This latter also took place during the reaction, since used CoMo-Ar-R displayed $Co^0$ and MoN, whereas used CoMo-Air-R showed $MoO_2$, $Co_3Mo_3N$ and Co-Mo oxynitride. The presence of $Co_3Mo_3N$ led to a higher activity (74.3% of ammonia at 650 °C and 36000 mL-$NH_3$ $g_{cat}^{-1}\ h^{-1}$) and stability. These authors affirmed that the prenitridation treatments (higher temperature prenitridation) allowed to generate $Co_3Mo_3N$ as the active phase, without other metal oxides, and a higher surface area (although this area was not the key issue to increase the activity).

In order to improve the activity of $Co_3Mo_3N$ materials, the influence of the addition of Cs has to this material on ammonia decomposition was studied in detail [93]. The synthesis method was carried out by a decomposition of hexamethylenetetramine (HMTA), Co, Ce and Mo salts under nitrogen a 700 °C. It was corroborated that Cs dispersed highly over $Co_3Mo_3N$ improving its electronic state. This upgrading provided hydrogen and nitrogen desorption, and thus, the reaction mechanism was accelerated.

In other work, $Co_3Mo_3N$, $Ni_3Mo_3N$ and $Fe_3Mo_3N$ were successfully prepared by temperature-programmed reaction of the corresponding oxide precursors with ammonia [94]. In spite of the small surface area (< 10 $m^2$ $g^{-1}$) and big crystallite size (> 10 nm) generated, these materials showed a suitable performance on the ammonia decomposition reaction. Three catalysts exhibited an ammonia conversion > 50 % at 550 °C, being the $Co_3Mo_3N$ catalyst that presented the lowest apparent activation energy (Ea = 70.0 kJ $mol^{-1}$). As mentioned above, $Co_3Mo_3N$ had an adequate N binding energy, justifying this behavior.

**Table 2**. Catalytic activity of non-noble catalysts for $H_2$ production from $NH_3$ decomposition performance at 1 atm.

| Catalysts | Metal loading (wt.%) | $S_{BET}$ ($m^2$ $g^{-1}$) | GHSV ($mL \cdot g_{cat}^{-1} \cdot h^{-1}$) | $NH_3$ inlet flow (%) | T (°C) | $NH_3$ conversion (%) | $H_2$ formation rate (mmol $H_2$ $g_{cat}^{-1}$ $min^{-1}$) | Ref. |
|---|---|---|---|---|---|---|---|---|
| 5Co/SiC | 5.0 | 24.0 | 60000 | 5 | 350 | 27.20 | 0.90 | [42] |
| 1Ca-5Co/SiC | 5.0 | 29.0 | 60000 | 5 | 350 | 22.80 | 0.76 | |
| 1Mg-5Co/SiC | 5.0 | 30.0 | 60000 | 5 | 350 | 29.60 | 0.99 | |
| 1La-5Co/SiC | 5.0 | 24.0 | 60000 | 5 | 350 | 27.40 | 0.92 | |
| 1K-5Co/SiC | 5.0 | 19.0 | 60000 | 5 | 350 | 33.10 | 1.12 | |
| 1Cs-5Co/SiC | 5.0 | 17.0 | 60000 | 5 | 350 | 25.10 | 0.84 | |
| 1Ce-5Co/SiC | 5.0 | 24.0 | 60000 | 5 | 350 | 20.30 | 0.68 | |
| 0.5K-5Co/SiC | 5.0 | 16.0 | 60000 | 5 | 350 | 31.90 | 1.07 | |
| 1.5K-5Co/SiC | 5.0 | 15.0 | 60000 | 5 | 350 | 28.50 | 0.95 | |
| Ni-Ca/$Y_2O_3$ | 40.0 | 32.0 | 6000 | 100 | 500 | 44.00 | 2.95 | [73] |
| 10Ni/$La_2O_3$-450 | 10.0 | 25.0 | 30000 | 100 | 550 | 59.0 | 19.75 | [74] |
| 10Ni/$La_2O_3$-550 | 10.0 | 23.0 | 30000 | 100 | 550 | 79.0 | 26.45 | |
| 10Ni/$La_2O_3$-650 | 10.0 | 14.0 | 30000 | 100 | 550 | 60.0 | 20.09 | |
| 10Ni/$La_2O_3$-750 | 10.0 | 11.0 | 30000 | 100 | 550 | 60.0 | 20.09 | |
| 10Ni/$La_2O_3$-850 | 10.0 | 10.0 | 30000 | 100 | 550 | 50.0 | 16.74 | |
| $LaNiO_3$ | - | 1.0 | 30000 | 100 | 550 | 60.0 | 20.09 | |
| 40Ni/5MgLa | 40.0 | 11.0 | 30000 | 100 | 550 | 82.0 | 27.46 | |
| Ni/$Y_2O_3$ | 10.0 | 7.0 | 6000 | 100 | 450 | 18.00 | 1.21 | [75] |
| Ni/$La_2O_3$ | 10.0 | 5.0 | 6000 | 100 | 450 | 12.00 | 0.80 | |
| Ni/$CeO_2$ | 10.0 | 4.0 | 6000 | 100 | 450 | 5.00 | 0.33 | |
| Ni/$Sm_2O_3$ | 10.0 | 9.0 | 6000 | 100 | 450 | 15.00 | 1.00 | |
| Ni/$Gd_2O_3$ | 10.0 | 4.0 | 6000 | 100 | 450 | 17.00 | 1.14 | |
| 5CMLa-$N_2$ | 5.0 | 33.0 | 6000 | 100 | 450 | 30.0 | 2.01 | [76] |

**Table 2.** Continued.

| Catalysts | Metal loading (wt.%) | $S_{BET}$ ($m^2$ $g^{-1}$) | GHSV ($mL \cdot g_{cat}^{-1} \cdot h^{-1}$) | $NH_3$ inlet flow (%) | T (°C) | $NH_3$ conversion (%) | $H_2$ formation rate (mmol $H_2$ $g_{cat}^{-1}$ $min^{-1}$) | Ref. |
|---|---|---|---|---|---|---|---|---|
| Co/$CeO_2$-nanocubes | 5.0 | 20.0 | 6000 | 100 | 550 | 67.0 | 4.49 | [77] |
| 1 $LaNiO_3$ 650 | - | 11.7 | 75000 | 5 | 350 | 55.90 | 2.34 | [43] |
| 0.5 $LaNiO_3$ 650 | - | 8.7 | 75000 | 5 | 350 | 36.70 | 1.54 | |
| 0.75 $LaNiO_3$ 650 | - | 9.0 | 75000 | 5 | 350 | 48.30 | 2.02 | |
| 1.25 $LaNiO_3$ 650 | - | 9.9 | 75000 | 5 | 350 | 33.60 | 1.41 | |
| 1 $LaNiO_3$ 700 | - | 9.7 | 75000 | 5 | 350 | 51.40 | 2.15 | |
| 1 $LaNiO_3$ 750 | - | 7.8 | 75000 | 5 | 350 | 41.60 | 1.74 | |
| 1 $LaNiO_3$ 900 | - | 3.2 | 75000 | 5 | 350 | 30.20 | 1.26 | |
| 1 $LaCoO_3$ 650 | - | 10.3 | 75000 | 5 | 350 | 44.70 | 1.87 | |
| 2 $LaCoO_3$ 700 | - | 13.4 | 75000 | 5 | 350 | 41.80 | 1.75 | |
| 3 $LaCoO_3$ 750 | - | 13.2 | 75000 | 5 | 350 | 38.20 | 1.60 | |
| 4 $LaCoO_3$ 900 | - | 3.5 | 75000 | 5 | 350 | 34.00 | 1.42 | |
| $LaNi_{80}Co_{20}O_3$ | - | 12.0 | 75000 | 5 | 350 | 30.00 | 1.26 | [44] |
| $LaNi_{60}Co_{40}O_3$ | - | 12.0 | 75000 | 5 | 350 | 31.70 | 1.33 | |
| $LaNi_{40}Co_{60}O_3$ | - | 9.0 | 75000 | 5 | 350 | 41.10 | 1.72 | |
| $LaNi_{20}Co_{80}O_3$ | - | 9.0 | 75000 | 5 | 350 | 37.10 | 1.55 | |
| $La_{90}Ce_{10}NiO_3$ | - | 11.0 | 75000 | 5 | 350 | 33.20 | 1.39 | |
| $La_{10}Ce_{90}NiO_3$ | - | 29.0 | 75000 | 5 | 350 | 59.10 | 2.47 | |
| $CeNiO_3$ | - | 15.0 | 75000 | 5 | 350 | 46.80 | 1.96 | |
| $La_{90}Mg_{10}NiO_3$ | - | 14.0 | 75000 | 5 | 350 | 37.70 | 1.58 | |
| $La_{10}Mg_{90}NiO_3$ | - | 25.0 | 75000 | 5 | 350 | 72.30 | 3.03 | |
| $MgNiO_3$ | - | 22.0 | 75000 | 5 | 350 | 43.00 | 1.80 | |

690

**Table 2.** Continued.

| Catalysts | Metal loading (wt.%) | $S_{BET}$ ($m^2$ $g^{-1}$) | GHSV ($mL \cdot g_{cat}^{-1} \cdot h^{-1}$) | $NH_3$ inlet flow (%) | T (°C) | $NH_3$ conversion (%) | $H_2$ formation rate (mmol $H_2$ $g_{cat}^{-1}$ $min^{-1}$) | Ref. |
|---|---|---|---|---|---|---|---|---|
| La-Co | - | 16.0 | 6000 | 100 | 350 | 4.00 | 0.27 | [80] |
| La-Ni | - | 20.0 | 6000 | 100 | 350 | 10.00 | 0.67 | |
| La-Ce-Co | - | 22.0 | 6000 | 100 | 350 | 4.00 | 0.27 | |
| 5Co-MgCeO | 5.0 | 16.2 | 6000 | 100 | 550 | 35.0 | 3.86 | [81] |
| 5Co-CaCeO | 5.0 | 11.0 | 6000 | 100 | 550 | 55.2 | 4.53 | |
| 5Co-SrCeO | 5.0 | 12.5 | 6000 | 100 | 550 | 41.1 | 4.67 | |
| 5Co-BaCeO | 5.0 | 15.7 | 6000 | 100 | 500 | 45.3 | 5.40 | |
| $Ni/Nb_2O_5$ | 40.0 | 7.4 | 6000 | 100 | 550 | 34.0 | 2.34 | [82] |
| $Ni/NaNbO_3$ | 40.0 | 4.1 | 6000 | 100 | 550 | 40.0 | 2.68 | |
| $Ni/KNbO_3$ | 40.0 | 8.4 | 6000 | 100 | 550 | 36.0 | 2.41 | |
| $Ni/LaAlO_3$ | 40.0 | 9.9 | 6000 | 100 | 550 | 65.0 | 4.35 | |
| $Ni/SmAlO_3$ | 40.0 | 8.1 | 6000 | 100 | 550 | 83.0 | 5.56 | |
| $Ni/GdAlO_3$ | 40.0 | 4.6 | 6000 | 100 | 550 | 83.0 | 5.56 | |
| $Ni/MnO_2$ | 40.0 | 2.4 | 6000 | 100 | 550 | 44.0 | 2.95 | |
| $Ni/CaMnO_3$ | 40.0 | 6.6 | 6000 | 100 | 550 | 55.0 | 3.68 | |
| $Ni/SrMnO_3$ | 40.0 | 7.9 | 6000 | 100 | 550 | 50.0 | 3.35 | |
| $Ni/BaMnO_3$ | 40.0 | 7.2 | 6000 | 100 | 550 | 47.0 | 3.15 | |
| $Ni/TiO_2$ | 40.0 | 12 | 6000 | 100 | 550 | 33.0 | 2.21 | |
| $Ni/CaTiO_2$ | 40.0 | 6.5 | 6000 | 100 | 550 | 37.0 | 2.48 | |
| $Ni/SrTiO_2$ | 40.0 | 5.5 | 6000 | 100 | 550 | 80.0 | 5.36 | |
| $Ni/BaTiO_2$ | 40.0 | 4.9 | 6000 | 100 | 550 | 75.0 | 5.02 | |
| $Ni/ZrO_2$ | 40.0 | 15.0 | 6000 | 100 | 550 | 27.0 | 1.81 | |
| $Ni/CaZrO_3$ | 40.0 | 6.0 | 6000 | 100 | 550 | 50.0 | 3.35 | |
| $Ni/SrZrO_3$ | 40.0 | 6.1 | 6000 | 100 | 550 | 93.0 | 6.03 | |
| $Ni/BaZrO_3$ | 40.0 | 7.5 | 6000 | 100 | 550 | 95.0 | 6.36 | |

**Table 2.** Continued.

| Catalysts | Metal loading (wt.%) | $S_{BET}$ ($m^2$ $g^{-1}$) | GHSV ($mL \cdot g_{cat}^{-1} \cdot h^{-1}$) | $NH_3$ inlet flow (%) | T (°C) | $NH_3$ conversion (%) | $H_2$ formation rate (mmol $H_2$ $g_{cat}^{-1}$ $min^{-1}$) | Ref. |
|---|---|---|---|---|---|---|---|---|
| Ni/Mg-Al-O | 20.0 | 4.7 | 6000 | 100 | 450 | 6.7 | 0.45 | [50] |
| Ni/Ca-Al-O | 20.0 | 16.7 | 6000 | 100 | 450 | 11.5 | 0.77 | |
| Ni/Sr-Al-O | 20.0 | 24.4 | 6000 | 100 | 450 | 16.5 | 1.10 | |
| Ni/Ba-Al-O | 20.0 | 15.0 | 6000 | 100 | 450 | 24.8 | 1.66 | |
| $Ni/Ca_2Al_1$-LDHs-ST | 23.6 | 30.1 | 10000 | 100 | 550 | 55.0 | 3.68 | [83] |
| $Ni/Ca_2Al_1$-LDHs-IM | 23.6 | 13.5 | 10000 | 100 | 550 | 25.0 | 1.67 | |
| Co/CZY | 10.0 | 30.0 | 6000 | 100 | 350 | 6.5 | 0.44 | [84] |
| Ni/CZY | 10.0 | 28.0 | 6000 | 100 | 350 | 6.0 | 0.40 | |
| $Ni_1Co_9$/CZY | 10.0 | 23.6 | 6000 | 100 | 350 | 10.5 | 0.70 | |
| 20Ni/MS | 20.0 | 20.0 | 30000 | 100 | 650 | 95.1 | 31.84 | [85] |
| 30Ni/MS | 22.0 | 30.0 | 30000 | 100 | 650 | 94.8 | 31.74 | |
| Ni-50/ATP | 5.8 | 38.6 | 30000 | 100 | 650 | 89.9 | 9.03 | [86] |
| Co-$Mg_3N_2$ | 5.4 | 12.0 | 36000 | 100 | 500 | 15.0 | 6.03 | [87] |
| Co-CaNH | 5.2 | 34.5 | 36000 | 100 | 500 | 38.0 | 15.27 | |
| Co-BaNH | 4.8 | 11.8 | 36000 | 100 | 500 | 50.0 | 20.09 | |
| 100Co | - | 25.0 | 18000 | 100 | 550 | 18.0 | 3.62 | [88] |
| NiO | - | 25.0 | 18000 | 100 | 550 | 3.0 | 0.60 | [89] |
| NiO | - | 18.7 | 12000 | 100 | 500 | 1.0 | 0.00 | [90] |
| Fe@CF(5) | 4.4 | 19.0 | 36000 | 100 | 550 | 5.0 | 2.01 | [91] |
| Fe@CF(10) | 8.0 | 19.6 | 36000 | 100 | 550 | 7.0 | 2.81 | |
| Fe@CF(15) | 13.5 | 21.1 | 36000 | 100 | 550 | 12.0 | 4.82 | |
| Mo@CF(10) | 7.0 | 19.7 | 36000 | 100 | 550 | 3.0 | 1.21 | |
| Mo@CF(15) | 12.5 | 22.7 | 36000 | 100 | 550 | 4.0 | 1.61 | |
| CoMo-Ar-R | - | 21.0 | 36000 | 100 | 650 | 71.2 | 28.61 | [92] |
| CoMo-Air-R | - | 23.7 | 36000 | 100 | 650 | 73.4 | 29.49 | |

**Table 2.** Continued.

| Catalysts | Metal loading (wt.%) | $S_{BET}$ ($m^2$ $g^{-1}$) | GHSV ($mL \cdot g_{cat}^{-1} \cdot h^{-1}$) | $NH_3$ inlet flow (%) | T (°C) | $NH_3$ conversion (%) | $H_2$ formation rate (mmol $H_2$ $g_{cat}^{-1}$ $min^{-1}$) | Ref. |
|---|---|---|---|---|---|---|---|---|
| Cs-$Co_3Mo_3N$ | - | 8.2 | 6000 | 100 | 450 | 48.0 | 3.21 | [93] |
| $Co_3Mo_3N$ | - | 6.1 | 6000 | 100 | 450 | 30.0 | 2.01 | |
| $Ni_3Mo_3N$ | - | 2.2 | 6000 | 100 | 450 | 18.0 | 1.21 | [94] |
| $Fe_3Mo_3N$ | - | 8.8 | 6000 | 100 | 450 | 16.0 | 1.07 | |

Therefore, a high surface area is usually thought to be a positive factor to disperse metals, resulting in larger number of active sites, and assisting mass transfer of the reaction [14,31,34,55,77,95]. In contrast, it is found that the utilization of precursors, mainly perovskites or hydrotalcites, could help to control the metal size to be small, providing high dispersion. In addition, the oxygen vacancies improve the electronic state of the metal active phase as well as the metal-support interaction, preferred by lower electronegative elements. Another factor that might reduce the reaction temperature is the application of carbide species, such as the novel SiC or $Fe_2C$ or $Mo_2C$. All of them allow the development of suitable catalysts with small surface area but suitable catalytic properties for the hydrogen generation from ammonia.

## 5. Conclusions and Future Prospects

Thermal decomposition of ammonia is an efficient technology to generate $CO_x$-free hydrogen and it is established as an important factor on the development of ammonia as a 'hydrogen carrier'. The design of an active catalyst to reduce the reaction temperature is one the central pillars of this technology. However, the catalytic activity is not only influenced by the metal active phase, but also, by the support, the addition of promoters as well as by the synthesis method. Despite of the high surface area supports improve the metal dispersion; this review provides a current perception on materials with small surface area. These materials show attractive results on hydrogen production from ammonia. The modification of the chemical and morphological properties of the active phase with basic and conductive supports led to a suitable performance, despite of their low porosity.

On the other hand, the utilization of precursors seems to be an original strategy to develop catalysts with small particle size, yielding an excellent ammonia conversion at low temperature. Additionally, chemical elements with smaller electronegativity are preferred to enhance the activity and increase reaction kinetics favoring the rate-determining step.

The use of non-noble metal catalysts, low-cost and eco-friendly supports could decrease the operation cost and reduce the reaction temperature, as well as increase the sustainability of the process. In addition, the utilization of other non-noble metals, different to nickel, cobalt, molybdenum, and iron, must be further investigated. The synthesis method should be optimized to reduce the time and cost, taking into account the importance of the sustainability of the process. In situ characterization techniques could help to verify the difference in the catalytic surface, whereas operando methods will assist to know the behavior of the catalysts during of ammonia decomposition reaction.

The utilization of carbide materials such as SiC or MoC should be explored and studied as catalytic supports for ammonia decomposition reaction. Additionally, $ABO_3$ formulations might enhance the ammonia conversion at low reaction temperature. The different combinations of mono and bimetallic perovskite-type oxides could promote the development of ammonia decomposition catalysts.

**Author Contributions:** M. P.: Investigation, Methodology, Validation, Visualization and Writing-Original draft preparation. P. S., A. R. d.l. O., A. R. and A. d. L.-C.: Conceptualization, Visualization, Writing-Reviewing, Supervision, Funding Acquisition. All authors have read and agreed to the published version of the manuscript.

**Funding:** This work was funded by the "Junta de Comunidades de Castilla-La Mancha (JCCM)" and European Union [FEDER funds SBPLY/21/180501/000165] and the UCLM (2022-PRED-20658).

**Data Availability Statement:** Not applicable.

**Acknowledgments:** Authors thank the "Junta de Comunidades de Castilla-La Mancha (JCCM)" and European Union [FEDER funds SBPLY/21/180501/000165]. M. Pinzón thanks the University of Castilla-La Mancha for the predoctoral contract within the framework of the Plan Propio I+D+I (2022-PRED-20658).

**Conflicts of Interest:** The authors declare no conflict of interest.

## References


1. Madurai Elavarasan, R.; Pugazhendhi, R.; Irfan, M.; Mihet-Popa, L.; Khan, I.A.; Campana, P.E. State-of-the-Art Sustainable Approaches for Deeper Decarbonization in Europe – An Endowment to Climate Neutral Vision. *Renew. Sustain. Energy Rev.* 2022, *159*, 112204.
2. Liu, Z.; Deng, Z.; He, G.; Wang, H.; Zhang, X.; Lin, J.; Qi, Y.; Liang, X. Challenges and Opportunities for Carbon Neutrality in China. *Nat. Rev. Earth Environ.* 2022, *3*, 141–155.
3. Capurso, T.; Stefanizzi, M.; Torresi, M.; Camporeale, S.M. Perspective of the Role of Hydrogen in the 21st Century Energy Transition. *Energy Convers. Manag.* 2022, *251*, 114898.
4. Niaz, S.; Manzoor, T.; Pandith, A.H. Hydrogen Storage: Materials, Methods and Perspectives. *Renew. Sustain. Energy Rev.* **2015**, *50*, 457–469, doi:10.1016/j.rser.2015.05.011.
5. Bockris, J.O. m.; Veziroglu, T.N. A Solar-Hydrogen Energy System for Environmental Compatibility. *Environ. Conserv.* **1985**, *12*, 105–118, doi:10.1017/S0376892900015526.
6. Osman, A.I.; Mehta, N.; Elgarahy, A.M.; Hefny, M.; Al-Hinai, A.; Ala', ·; Al-Muhtaseb, H.; David, ·; Rooney, W. Hydrogen Production, Storage, Utilisation and Environmental Impacts: A Review. **2022**, *20*, 153–188, doi:10.1007/s10311-021-01322-8.
7. Kapdan, I.K.; Kargi, F. Bio-Hydrogen Production from Waste Materials. *Enzyme Microb. Technol.* **2006**, *38*, 569–582, doi:10.1016/j.enzmictec.2005.09.015.
8. Bockris, J.O.M. The Hydrogen Economy: Its History. *Int. J. Hydrogen Energy* **2013**, *38*, 2579–2588, doi:10.1016/J.IJHYDENE.2012.12.026.
9. Hosseini, S.E.; Wahid, M.A. Hydrogen Production from Renewable and Sustainable Energy Resources: Promising Green Energy Carrier for Clean Development. *Renew. Sustain. Energy Rev.* **2016**, *57*, 850–866, doi:10.1016/j.rser.2015.12.112.
10. Bassani, A.; Previtali, D.; Pirola, C.; Bozzano, G.; Colombo, S.; Manenti, F. Mitigating Carbon Dioxide Impact of Industrial Steam Methane Reformers by Acid Gas to Syngas Technology: Technical and Environmental Feasibility. *J. Sustain. Dev. Energy, Water Environ. Syst.* **2020**, *8*, 71–87, doi:10.13044/j.sdewes.d7.0258.
11. Dawood, F.; Anda, M.; Shafiullah, G.M. Hydrogen Production for Energy: An Overview. *Int. J. Hydrogen Energy* **2020**, *45*, 3847–3869, doi:10.1016/j.ijhydene.2019.12.059.
12. Pawelczyk, E.; Łukasik, N.; Wysocka, I.; Rogala, A.; G¸ Ebicki, J. Recent Progress on Hydrogen Storage and Production Using Chemical Hydrogen Carriers. *Energies 2022, Vol. 15, Page 4964* **2022**, *15*, 4964, doi:10.3390/EN15144964.
13. Zheng, J.; Zhou, H.; Wang, C.G.; Ye, E.; Xu, J.W.; Loh, X.J.; Li, Z. Current Research Progress and Perspectives on Liquid Hydrogen Rich Molecules in Sustainable Hydrogen Storage. *Energy Storage Mater.* **2021**, *35*, 695–722, doi:10.1016/J.ENSM.2020.12.007.
14. Lucentini, I.; Garcia, X.; Vendrell, X.; Llorca, J. Review of the Decomposition of Ammonia to Generate Hydrogen. *Ind. Eng. Chem. Res.* **2021**, *60*, 18560–18611, doi:10.1021/acs.iecr.1c00843.
15. Lamb, K.E.; Dolan, M.D.; Kennedy, D.F. Ammonia for Hydrogen Storage; A Review of Catalytic Ammonia Decomposition and Hydrogen Separation and Purification. *Int. J. Hydrogen Energy* **2019**, *44*, 3580–3593, doi:10.1016/j.ijhydene.2018.12.024.
16. Cesaro, Z.; Ives, M.; Nayak-Luke, R.; Mason, M.; Bañares-Alcántara, R. Ammonia to Power: Forecasting the Levelized Cost of Electricity from Green Ammonia in Large-Scale Power Plants. *Appl. Energy* **2021**, *282*, doi:10.1016/j.apenergy.2020.116009.
17. Ristig, S.; Poschmann, M.; Folke, J.; Gómez-Cápiro, O.; Chen, Z.; Sanchez-Bastardo, N.; Schlögl, R.; Heumann, S.; Ruland, H. Ammonia Decomposition in the Process Chain for a Renewable Hydrogen Supply. *Chemie Ing. Tech.* **2022**, doi:10.1002/cite.202200003.
18. Chehade, G.; Dincer, I. Progress in Green Ammonia Production as Potential Carbon-Free Fuel. *Fuel* 2021, *299*, 120845.
19. Valera-Medina, A.; Amer-Hatem, F.; Azad, A.K.; Dedoussi, I.C.; De Joannon, M.; Fernandes, R.X.; Glarborg, P.; Hashemi, H.; He, X.; Mashruk, S.; et al. Review on Ammonia as a Potential Fuel: From Synthesis to Economics. *Energy and Fuels* 2021, *35*,

6964–7029.

20. Aziz, M.; TriWijayanta, A.; Nandiyanto, A.B.D. Ammonia as Effective Hydrogen Storage: A Review on Production, Storage and Utilization. *Energies* **2020**, *13*, 1–25, doi:10.3390/en13123062.
21. Arnaiz del Pozo, C.; Cloete, S. Techno-Economic Assessment of Blue and Green Ammonia as Energy Carriers in a Low-Carbon Future. *Energy Convers. Manag.* **2022**, *255*, 115312, doi:10.1016/j.enconman.2022.115312.
22. Morlanés, N.; Katikaneni, S.P.; Paglieri, S.N.; Harale, A.; Solami, B.; Sarathy, S.M.; Gascon, J. A Technological Roadmap to the Ammonia Energy Economy: Current State and Missing Technologies. *Chem. Eng. J.* **2021**, *408*, 127310, doi:10.1016/j.cej.2020.127310.
23. Wan, Z.; Tao, Y.; Shao, J.; Zhang, Y.; You, H. Ammonia as an Effective Hydrogen Carrier and a Clean Fuel for Solid Oxide Fuel Cells. *Energy Convers. Manag.* **2021**, *228*, doi:10.1016/j.enconman.2020.113729.
24. López-Fernández, E.; Sacedón, C.G.; Gil-Rostra, J.; Yubero, F.; González-Elipe, A.R.; de Lucas-Consuegra, A. Recent Advances in Alkaline Exchange Membrane Water Electrolysis and Electrode Manufacturing. *Molecules* 2021, *26*, 6326.
25. Barisano, D.; Canneto, G.; Nanna, F.; Villone, A.; Fanelli, E.; Freda, C.; Grieco, M.; Lotierzo, A.; Cornacchia, G.; Braccio, G.; et al. Investigation of an Intensified Thermo-Chemical Experimental Set-Up for Hydrogen Production from Biomass: Gasification Process Integrated to a Portable Purification System—Part II. *Energies 2022, Vol. 15, Page 4580* **2022**, *15*, 4580, doi:10.3390/EN15134580.
26. Mutch, G.A. Electrochemical Separation Processes for Future Societal Challenges. *Cell Reports Phys. Sci.* 2022, *3*, 100844.
27. Smith, C.; Hill, A.K.; Torrente-Murciano, L. Current and Future Role of Haber-Bosch Ammonia in a Carbon-Free Energy Landscape. *Energy Environ. Sci.* **2020**, *13*, 331–344, doi:10.1039/c9ee02873k.
28. Soloveichik, G. Electrochemical Synthesis of Ammonia as a Potential Alternative to the Haber–Bosch Process. *Nat. Catal.* 2019, *2*, 377–380.
29. International Energy Agency The Future of Hydrogen – Analysis - IEA Available online: https://www.iea.org/reports/the-future-of-hydrogen (accessed on 3 November 2021).
30. Ciucci, M. Energy Policy: General Principles | Fact Sheets on the European Union Available online: https://www.europarl.europa.eu/factsheets/en/sheet/68/energy-policy-general-principles (accessed on 26 July 2022).
31. Mateti, S.; Saranya, L.; Sathikumar, G.; Cai, Q.; Yao, Y.; Chen, Y.I. Nanomaterials Enhancing the Solid-State Storage and Decomposition of Ammonia. *Nanotechnology* 2022, *33*, 222001.
32. García-Bordejé, E.; Armenise, S.; Roldán, L. Toward Practical Application Of H2 Generation From Ammonia Decomposition Guided by Rational Catalyst Design. *Catal. Rev.* **2014**, *56*, 220–237, doi:10.1080/01614940.2014.903637.
33. Armenise, S.; García-Bordejé, E.; Valverde, J.L.; Romeo, E.; Monzón, A. A Langmuir–Hinshelwood Approach to the Kinetic Modelling of Catalytic Ammonia Decomposition in an Integral Reactor. *Phys. Chem. Chem. Phys.* **2013**, *15*, 12104, doi:10.1039/c3cp50715g.
34. Le, T.A.; Do, Q.C.; Kim, Y.; Kim, T.W.; Chae, H.J. A Review on the Recent Developments of Ruthenium and Nickel Catalysts for COx-Free H2 Generation by Ammonia Decomposition. *Korean J. Chem. Eng.* 2021, *38*, 1087–1103.
35. Ganley, J.C.; Thomas, F.S.; Seebauer, E.G.; Masel, R.I. A Priori Catalytic Activity Correlations: The Difficult Case of Hydrogen Production from Ammonia. *Catal. Letters* **2004**, *96*, 117–122, doi:10.1023/B:CATL.0000030108.50691.d4.
36. Chellappa, A.S.; Fischer, C.M.; Thomson, W.J. Ammonia Decomposition Kinetics over Ni-Pt/Al2O3 for PEM Fuel Cell Applications. *Appl. Catal. A Gen.* **2002**, *227*, 231–240, doi:10.1016/S0926-860X(01)00941-3.
37. BOISEN, A.; DAHL, S.; NORSKOV, J.; CHRISTENSEN, C. Why the Optimal Ammonia Synthesis Catalyst Is Not the Optimal Ammonia Decomposition Catalyst. *J. Catal.* **2005**, *230*, 309–312, doi:10.1016/j.jcat.2004.12.013.
38. García-García, F.R.; Guerrero-Ruiz, A.; Rodríguez-Ramos, I. Role of B5-Type Sites in Ru Catalysts Used for the NH 3 Decomposition Reaction. *Top. Catal.* **2009**, *52*, 758–764, doi:10.1007/s11244-009-9203-7.

39. Karim, A.M.; Prasad, V.; Mpourmpakis, G.; Lonergan, W.W.; Frenkel, A.I.; Chen, J.G.; Vlachos, D.G. Correlating Particle Size and Shape of Supported Ru/γ-Al2O3 Catalysts with NH3 Decomposition Activity. *J. Am. Chem. Soc.* **2009**, *131*, 12230–12239, doi:10.1021/ja902587k.
40. Pinzón, M.; Romero, A.; de Lucas Consuegra, A.; de la Osa, A.R.; Sánchez, P. Hydrogen Production by Ammonia Decomposition over Ruthenium Supported on SiC Catalyst. *J. Ind. Eng. Chem.* **2021**, *94*, 326–335, doi:10.1016/j.jiec.2020.11.003.
41. Pinzón, M.; Avilés-García, O.; de la Osa, A.R.; de Lucas-Consuegra, A.; Sánchez, P.; Romero, A. New Catalysts Based on Reduced Graphene Oxide for Hydrogen Production from Ammonia Decomposition. *Sustain. Chem. Pharm.* **2022**, *25*, 100615, doi:10.1016/j.scp.2022.100615.
42. Pinzón, M.; Romero, A.; de Lucas-Consuegra, A.; de la Osa, A.R.; Sánchez, P. COx-Free Hydrogen Production from Ammonia at Low Temperature Using Co/SiC Catalyst: Effect of Promoter. *Catal. Today* **2022**, *390–391*, 34–47, doi:10.1016/j.cattod.2021.12.005.
43. Pinzón, M.; Sánchez-Sánchez, A.; Sánchez, P.; de la Osa, A.R.; Romero, A. Ammonia as a Carrier for Hydrogen Production by Using Lanthanum Based Perovskites. *Energy Convers. Manag.* **2021**, *246*, 114681, doi:10.1016/j.enconman.2021.114681.
44. Pinzón, M.; Sánchez-Sánchez, A.; Romero, A.; de la Osa, A.R.; Sánchez, P. Self-Combustion Ni and Co-Based Perovskites as Catalyst Precursors for Ammonia Decomposition. Effect of Ce and Mg Doping. *Fuel* **2022**, *323*, 124384, doi:10.1016/J.FUEL.2022.124384.
45. Li, Y.; Wen, J.; Ali, A.M.; Duan, M.; Zhu, W.; Zhang, H.; Chen, C.; Li, Y. Size Structure–Catalytic Performance Correlation of Supported Ni/MCF-17 Catalysts for CO x -Free Hydrogen Production. *Chem. Commun.* **2018**, *54*, 6364–6367, doi:10.1039/C8CC01884G.
46. Bell, T.E.; Ménard, H.; González Carballo, J.-M.; Tooze, R.; Torrente-Murciano, L. Hydrogen Production from Ammonia Decomposition Using Co/γ-Al2O3 Catalysts – Insights into the Effect of Synthetic Method. *Int. J. Hydrogen Energy* **2020**, *45*, 27210–27220, doi:10.1016/j.ijhydene.2020.07.090.
47. Duan, X.; Qian, G.; Liu, Y.; Ji, J.; Zhou, X.; Chen, D.; Yuan, W. Structure Sensitivity of Ammonia Decomposition over Ni Catalysts: A Computational and Experimental Study. *Fuel Process. Technol.* **2013**, *108*, 112–117, doi:10.1016/j.fuproc.2012.05.030.
48. Bell, T.E.; Torrente-Murciano, L. H2 Production via Ammonia Decomposition Using Non-Noble Metal Catalysts: A Review. *Top. Catal.* **2016**, *59*, 1438–1457, doi:10.1007/s11244-016-0653-4.
49. Hu, X.-C.; Wang, W.-W.; Jin, Z.; Wang, X.; Si, R.; Jia, C.-J. Transition Metal Nanoparticles Supported La-Promoted MgO as Catalysts for Hydrogen Production via Catalytic Decomposition of Ammonia. *J. Energy Chem.* **2019**, *38*, 41–49, doi:10.1016/j.jechem.2018.12.024.
50. Im, Y.; Muroyama, H.; Matsui, T.; Eguchi, K. Ammonia Decomposition over Nickel Catalysts Supported on Alkaline Earth Metal Aluminate for H2 Production. *Int. J. Hydrogen Energy* **2020**, *45*, 26979–26988, doi:10.1016/j.ijhydene.2020.07.014.
51. Zhao, Z.; Zou, H.; Lin, W. Effect of Rare Earth and Other Cationic Promoters on Properties of CoMoNx/CNTs Catalysts for Ammonia Decomposition. *J. Rare Earths* **2013**, *31*, 247–250, doi:10.1016/S1002-0721(12)60266-X.
52. Zheng, W.; Zhang, J.; Ge, Q.; Xu, H.; Li, W. Effects of CeO2 Addition on Ni/Al2O3 Catalysts for the Reaction of Ammonia Decomposition to Hydrogen. *Appl. Catal. B Environ.* **2008**, *80*, 98–105, doi:10.1016/j.apcatb.2007.11.008.
53. Mukherjee, S.; Devaguptapu, S. V.; Sviripa, A.; Lund, C.R.F.; Wu, G. Low-Temperature Ammonia Decomposition Catalysts for Hydrogen Generation. *Appl. Catal. B Environ.* **2018**, *226*, 162–181, doi:10.1016/j.apcatb.2017.12.039.
54. Sayas, S.; Morlanés, N.; Katikaneni, S.P.; Harale, A.; Solami, B.; Gascon, J. High Pressure Ammonia Decomposition on Ru-K/CaO Catalysts. *Catal. Sci. Technol.* **2020**, *10*, 5027–5035, doi:10.1039/d0cy00686f.
55. Sun, S.; Jiang, Q.; Zhao, D.; Cao, T.; Sha, H.; Zhang, C.; Song, H.; Da, Z. Ammonia as Hydrogen Carrier: Advances in Ammonia Decomposition Catalysts for Promising Hydrogen Production. *Renew. Sustain. Energy Rev.* **2022**, *169*, 112918,

doi:10.1016/J.RSER.2022.112918.

56. Hu, Z.; Mahin, J.; Datta, S.; Bell, T.E.; Torrente-Murciano, L. Ru-Based Catalysts for H2 Production from Ammonia: Effect of 1D Support. *Top. Catal.* **2019**, *62*, 1169–1177, doi:10.1007/s11244-018-1058-3.
57. Furusawa, T.; Kuribara, H.; Kimura, K.; Sato, T.; Itoh, N. Development of a Cs-Ru/CeO2 Spherical Catalyst Prepared by Impregnation and Washing Processes for Low-Temperature Decomposition of NH3: Characterization and Kinetic Analysis Results. *Ind. Eng. Chem. Res.* **2020**, *59*, 18460–18470, doi:10.1021/acs.iecr.0c03112.
58. Huang, C.; Yu, Y.; Yang, J.; Yan, Y.; Wang, D.; Hu, F.; Wang, X.; Zhang, R.; Feng, G. Ru/La2O3 Catalyst for Ammonia Decomposition to Hydrogen. *Appl. Surf. Sci.* **2019**, *476*, 928–936, doi:10.1016/j.apsusc.2019.01.112.
59. Im, Y.; Muroyama, H.; Matsui, T.; Eguchi, K. Investigation on Catalytic Performance and Desorption Behaviors of Ruthenium Catalysts Supported on Rare-Earth Oxides for NH3 Decomposition. *Int. J. Hydrogen Energy* **2022**, doi:10.1016/J.IJHYDENE.2022.07.162.
60. Feng, J.; Zhang, X.; Wang, J.; Ju, X.; Liu, L.; Chen, P. Applications of Rare Earth Oxides in Catalytic Ammonia Synthesis and Decomposition. *Catal. Sci. Technol.* 2021, *11*, 6330–6343.
61. Muroyama, H.; Matsui, T.; Eguchi, K. Production and Utilization of Hydrogen Carriers by Using Supported Nickel Catalysts. *J. Japan Pet. Inst.* **2021**, *64*, 123–131, doi:10.1627/jpi.64.123.
62. Zhang, X.; Liu, L.; Feng, J.; Ju, X.; Wang, J.; He, T.; Chen, P. Metal–Support Interaction-Modulated Catalytic Activity of Ru Nanoparticles on Sm2O3 for Efficient Ammonia Decomposition. *Catal. Sci. Technol.* **2021**, *11*, 2915–2923, doi:10.1039/D1CY00080B.
63. Le, T.A.; Kim, Y.; Kim, H.W.; Lee, S.U.; Kim, J.R.; Kim, T.W.; Lee, Y.J.; Chae, H.J. Ru-Supported Lanthania-Ceria Composite as an Efficient Catalyst for COx-Free H2 Production from Ammonia Decomposition. *Appl. Catal. B Environ.* **2021**, *285*, 119831, doi:10.1016/j.apcatb.2020.119831.
64. Doh, H.; Kim, H.Y.; Kim, G.S.; Cha, J.; Park, H.S.; Ham, H.C.; Yoon, S.P.; Han, J.; Nam, S.W.; Song, K.H.; et al. Influence of Cation Substitutions Based on ABO3 Perovskite Materials, Sr1-XYxTi1-YRuyO3-δ, on Ammonia Dehydrogenation. *ACS Sustain. Chem. Eng.* **2017**, *5*, 9370–9379, doi:10.1021/acssuschemeng.7b02402.
65. Cao, C.F.; Wu, K.; Zhou, C.; Yao, Y.H.; Luo, Y.; Chen, C.Q.; Lin, L.; Jiang, L. Electronic Metal-Support Interaction Enhanced Ammonia Decomposition Efficiency of Perovskite Oxide Supported Ruthenium. *Chem. Eng. Sci.* **2022**, *257*, 117719, doi:10.1016/j.ces.2022.117719.
66. Zhiqiang, F.; Ziqing, W.; Dexing, L.; Jianxin, L.; Lingzhi, Y.; Qin, W.; Zhong, W. Catalytic Ammonia Decomposition to COx-Free Hydrogen over Ruthenium Catalyst Supported on Alkali Silicates. *Fuel* **2022**, *326*, 125094, doi:10.1016/j.fuel.2022.125094.
67. Zhao, J.; Xu, S.; Wu, H.; You, Z.; Deng, L.; Qiu, X. Metal-Support Interactions on Ru/CaAlO: X Catalysts Derived from Structural Reconstruction of Ca-Al Layered Double Hydroxides for Ammonia Decomposition. *Chem. Commun.* **2019**, *55*, 14410–14413, doi:10.1039/c9cc05706d.
68. Wang, Z.; Qu, Y.; Shen, X.; Cai, Z. Ruthenium Catalyst Supported on Ba Modified ZrO2 for Ammonia Decomposition to COx-Free Hydrogen. *Int. J. Hydrogen Energy* **2019**, *44*, 7300–7307, doi:10.1016/j.ijhydene.2019.01.235.
69. Hu, Z.; Mahin, J.; Torrente-Murciano, L. A MOF-Templated Approach for Designing Ruthenium–Cesium Catalysts for Hydrogen Generation from Ammonia. *Int. J. Hydrogen Energy* **2019**, *44*, 30108–30118, doi:10.1016/j.ijhydene.2019.09.174.
70. Miyamoto, M.; Hamajima, A.; Oumi, Y.; Uemiya, S. Effect of Basicity of Metal Doped ZrO2 Supports on Hydrogen Production Reactions. *Int. J. Hydrogen Energy* **2018**, *43*, 730–738, doi:10.1016/j.ijhydene.2017.11.041.
71. Chung, D.B.; Kim, H.Y.; Jeon, M.; Lee, D.H.; Park, H.S.; Choi, S.H.; Nam, S.W.; Jang, S.C.; Park, J.H.; Lee, K.Y.; et al. Enhanced Ammonia Dehydrogenation over Ru/La(x)-Al2O3 (x = 0–50 Mol%): Structural and Electronic Effects of La Doping. *Int. J. Hydrogen Energy* **2017**, *42*, 1639–1647, doi:10.1016/j.ijhydene.2016.08.020.
72. Sayas, S.; Morlanés, N.; Katikaneni, S.P.; Harale, A.; Solami, B.; Gascon, J. High Pressure Ammonia Decomposition on Ru-

K/CaO Catalysts. *Catal. Sci. Technol.* **2020**, *10*, 5027–5035, doi:10.1039/d0cy00686f.

73. Okura, K.; Okanishi, T.; Muroyama, H.; Matsui, T.; Eguchi, K. Additive Effect of Alkaline Earth Metals on Ammonia Decomposition Reaction over Ni/Y2O3 Catalysts. *RSC Adv.* **2016**, *6*, 85142–85148, doi:10.1039/c6ra19005g.
74. Yu, Y.; Gan, Y.; Huang, C.; Lu, Z.; Wang, X.; Zhang, R.; Feng, G. Ni/La2O3 and Ni/MgO–La2O3 Catalysts for the Decomposition of NH3 into Hydrogen. *Int. J. Hydrogen Energy* **2020**, *45*, 16528–16539, doi:10.1016/j.ijhydene.2020.04.127.
75. Okura, K.; Okanishi, T.; Muroyama, H.; Matsui, T.; Eguchi, K. Ammonia Decomposition over Nickel Catalysts Supported on Rare-Earth Oxides for the On-Site Generation of Hydrogen. *ChemCatChem* **2016**, *8*, 2988–2995, doi:10.1002/cctc.201600610.
76. Podila, S.; Driss, H.; Zaman, S.F.; Alhamed, Y.A.; Alzahrani, A.A.; Daous, M.A.; Petrov, L.A. Hydrogen Generation by Ammonia Decomposition Using Co/MgO-La2O3 Catalyst: Influence of Support Calcination Atmosphere. *J. Mol. Catal. A Chem.* **2016**, *414*, 130–139, doi:10.1016/j.molcata.2016.01.012.
77. Huang, C.; Yu, Y.; Tang, X.; Liu, Z.; Zhang, J.; Ye, C.; Ye, Y.; Zhang, R. Hydrogen Generation by Ammonia Decomposition over Co/CeO2 Catalyst: Influence of Support Morphologies. *Appl. Surf. Sci.* **2020**, *532*, 147335, doi:10.1016/j.apsusc.2020.147335.
78. Okura, K.; Okanishi, T.; Muroyama, H.; Matsui, T.; Eguchi, K. Promotion Effect of Rare-Earth Elements on the Catalytic Decomposition of Ammonia over Ni/Al2O3 Catalyst. *Appl. Catal. A Gen.* **2015**, *505*, 77–85, doi:10.1016/j.apcata.2015.07.020.
79. Muroyama, H.; Saburi, C.; Matsui, T.; Eguchi, K. Ammonia Decomposition over Ni/La2O3 Catalyst for on-Site Generation of Hydrogen. *Appl. Catal. A Gen.* **2012**, *443–444*, 119–124, doi:10.1016/j.apcata.2012.07.031.
80. Podila, S.; Driss, H.; Ali, A.M.; Al-Zahrani, A.A.; Daous, M.A. Influence of Ce Substitution in LaMO3 (M = Co/Ni) Perovskites for COx-Free Hydrogen Production from Ammonia Decomposition. *Arab. J. Chem.* **2022**, *15*, 103547, doi:10.1016/J.ARABJC.2021.103547.
81. Al-attar, O.A.; Podila, S.; Al-Zahrani, A.A. Preparation and Study of XCeO3 (X: Mg, Ca, Sr, Ba) Perovskite-Type Oxide Supported Cobalt Catalyst for Hydrogen Production by Ammonia Decomposition. *Arab. J. Sci. Eng.* **2022**, 1–11, doi:10.1007/s13369-022-07255-w.
82. Okura, K.; Miyazaki, K.; Muroyama, H.; Matsui, T.; Eguchi, K. Ammonia Decomposition over Ni Catalysts Supported on Perovskite-Type Oxides for the on-Site Generation of Hydrogen. *RSC Adv.* **2018**, *8*, 32102–32110, doi:10.1039/c8ra06100a.
83. Zhao, J.; Deng, L.; Zheng, W.; Xu, S.; Yu, Q.; Qiu, X. Nickel-Induced Structure Transformation in Hydrocalumite for Enhanced Ammonia Decomposition. *Int. J. Hydrogen Energy* **2020**, *45*, 12244–12255, doi:10.1016/j.ijhydene.2020.02.201.
84. Huang, C.; Li, H.; Yang, J.; Wang, C.; Hu, F.; Wang, X.; Lu, Z.-H.; Feng, G.; Zhang, R. Ce0.6Zr0.3Y0.1O2 Solid Solutions-Supported Ni Co Bimetal Nanocatalysts for NH3 Decomposition. *Appl. Surf. Sci.* **2019**, *478*, 708–716, doi:10.1016/j.apsusc.2019.01.269.
85. Hu, Z.P.; Weng, C.C.; Yuan, G.G.; Lv, X.W.; Yuan, Z.Y. Ni Nanoparticles Supported on Mica for Efficient Decomposition of Ammonia to COx-Free Hydrogen. *Int. J. Hydrogen Energy* **2018**, *43*, 9663–9676, doi:10.1016/j.ijhydene.2018.04.029.
86. Li, L.; Chen, F.; Shao, J.; Dai, Y.; Ding, J.; Tang, Z. Attapulgite Clay Supported Ni Nanoparticles Encapsulated by Porous Silica: Thermally Stable Catalysts for Ammonia Decomposition to COx Free Hydrogen. *Int. J. Hydrogen Energy* **2016**, *41*, 21157–21165, doi:10.1016/j.ijhydene.2016.08.156.
87. Yu, P.; Wu, H.; Guo, J.; Wang, P.; Chang, F.; Gao, W.; Zhang, W.; Liu, L.; Chen, P. Effect of BaNH, CaNH, Mg3N2 on the Activity of Co in NH3 Decomposition Catalysis. *J. Energy Chem.* **2020**, *46*, 16–21, doi:10.1016/j.jechem.2019.10.014.
88. Zhang, Z.-S.; Fu, X.-P.; Wang, W.-W.; Jin, Z.; Song, Q.-S.; Jia, C.-J. Promoted Porous Co3O4-Al2O3 Catalysts for Ammonia Decomposition. *Sci. China Chem.* **2018**, *61*, 1389–1398, doi:10.1007/s11426-018-9261-5.
89. Yan, H.; Xu, Y.J.; Gu, Y.Q.; Li, H.; Wang, X.; Jin, Z.; Shi, S.; Si, R.; Jia, C.J.; Yan, C.H. Promoted Multimetal Oxide Catalysts for the Generation of Hydrogen via Ammonia Decomposition. *J. Phys. Chem. C* **2016**, *120*, 7685–7696, doi:10.1021/acs.jpcc.6b01595.
90. Nakamura, I.; Fujitani, T. Role of Metal Oxide Supports in NH 3 Decomposition over Ni Catalysts. *Appl. Catal. A Gen.* **2016**,

*524*, 45–49, doi:10.1016/j.apcata.2016.05.020.

91. Guler, M.; Korkusuz, C.; Varisli, D. Catalytic Decomposition of Ammonia for Hydrogen Production over Carbon Nanofiber Supported Fe and Mo Catalysts in a Microwave Heated Reactor. *Int. J. Chem. React. Eng.* **2019**, *17*, 1–13, doi:10.1515/ijcre-2018-0162.
92. Duan, X.; Ji, J.; Yan, X.; Qian, G.; Chen, D.; Zhou, X. Understanding Co-Mo Catalyzed Ammonia Decomposition: Influence of Calcination Atmosphere and Identification of Active Phase. *ChemCatChem* **2016**, *8*, 938–945, doi:10.1002/cctc.201501275.
93. Srifa, A.; Okura, K.; Okanishi, T.; Muroyama, H.; Matsui, T.; Eguchi, K. Hydrogen Production by Ammonia Decomposition over Cs-Modified Co3Mo3N Catalysts. *Appl. Catal. B Environ.* **2017**, *218*, 1–8, doi:10.1016/j.apcatb.2017.06.034.
94. Srifa, A.; Okura, K.; Okanishi, T.; Muroyama, H.; Matsui, T.; Eguchi, K. CO x -Free Hydrogen Production via Ammonia Decomposition over Molybdenum Nitride-Based Catalysts. *Catal. Sci. Technol.* **2016**, *6*, 7495–7504, doi:10.1039/C6CY01566B.
95. Chen, C.; Wu, K.; Ren, H.; Zhou, C.; Luo, Y.; Lin, L.; Au, C.; Jiang, L. Ru-Based Catalysts for Ammonia Decomposition: A Mini-Review. *Energy and Fuels* 2021, *35*, 11693–11706.